Small variations in nanoparticle structure dictate differential cellular stress responses and mode of cell death

Marzena Szwed[1, *], Tonje Sønstevold[1, 2, *], Anders Øverbye[1], Nikolai Engedal[3], Beata Grallert[4], Ýrr Mørch[5], Einar Sulheim[5, 6], Tore-Geir Iversen[1], Tore Skotland[1], Kirsten Sandvig[1, 2], Maria L Torgersen[1, †]

[1] *Department of Molecular Cell Biology, Institute for Cancer Research, Oslo University Hospital, Montebello, N-0379 Oslo, Norway.*

[2] *Department of Biosciences, Faculty of Mathematics and Natural Sciences, University of Oslo, 0316 Oslo, Norway.*

[3] *Centre for Molecular Medicine Norway (NCMM); Nordic EMBL Partnership; University of Oslo, Norway.*

[4] *Department of Radiation Biology, Institute for Cancer Research, Oslo University Hospital, Montebello, N-0379 Oslo, Norway.*

[5] *Department of Biotechnology and Nanomedicine, SINTEF AS, Sem Sælands vei 2A, 7034 Trondheim, Norway.*

[6] *Department of Physics, Faculty of Natural Sciences, The Norwegian University of Science and Technology (NTNU), Trondheim, Norway.*

[*] These authors contributed equally to this work; [†] Corresponding author.

For correspondence: Maria L. Torgersen, Department of Molecular Cell Biology, Institute for Cancer Research, Oslo University Hospital, Montebello, N-0379 Oslo, Norway. Tel: +47 22 78 18 26; Fax: +47 22 78 18 45; e-mail: marialy@rr-research.no

Abstract

For optimal exploitation of nanoparticles (NPs) in biomedicine, and to predict nanotoxicity, detailed knowledge of the cellular responses to cell-bound or internalized NPs is imperative. The final outcome of NP-cell interaction is dictated by the type and magnitude of the NP insult and the cellular response. Here, this has been systematically studied by using poly(alkylcyanoacrylate) (PACA) particles differing only in their alkyl side chains; butyl (PBCA), ethylbutyl (PEBCA), or octyl (POCA), respectively. Surprisingly, these highly similar NPs induced different stress responses and modes of cell death in human cell lines. The POCA particles generally induced endoplasmic reticulum stress and apoptosis. In contrast, PBCA and PEBCA particles induced oxidative stress and lipid peroxidation depending on the level of the glutathione precursor cystine and transcription of the cystine transporter SLC7A11. The latter was induced as a protective response by the transcription factors ATF4 and Nrf2. PBCA particles strongly activated ATF4 downstream of the eIF2α kinase HRI, whereas PEBCA particles more potently induced Nrf2 antioxidant responses. Intriguingly, PBCA particles activated the cell death mechanism ferroptosis; a promising option for targeting multidrug-resistant cancers. Our findings highlight that even minor differences in NP composition can severely impact the cellular response to NPs. This may have important implications in therapeutic settings.

Poly(alkylcyanoacrylate), ER stress, oxidative stress, integrated stress response, ferroptosis.

Introduction

The fact that many normally 'inert' materials become substantially more reactive when downsized to nanoparticles (NPs) can be exploited in nanomedicine (Peynshaert et al. 2014), but also give rise to nanotoxicity (Higashisaka et al. 2017). Intracellular uptake of NPs into lysosomes, or even NP binding to the cell surface, has been shown to activate cellular stress responses, such as oxidative stress or endoplasmic reticulum (ER) stress (Abdal Dayem et al. 2017; Cao et al. 2017; Sukhanova et al. 2018) (Figure 1A). In NP-mediated drug delivery, cellular stress pathways that are induced as a response to the nanocarrier itself may be beneficial if these stress responses sensitize the target cells to the intended drug effect. A variety of NPs have been shown to alter the cellular redox balance either by overproduction of reactive oxygen species (ROS) or by depleting the cellular reserve of the main ROS scavenger molecule, reduced glutathione (GSH) (Abdal Dayem et al. 2017). To regain redox homeostasis, an antioxidant response is initiated by activation of transcription factors like Nrf2, HIF1, NFκB, or ATF4, which induce expression of proteins with antioxidant properties (Bellezza et al. 2018; Sies et al. 2017). ER stress is characterized by disruption of ER lumen homeostasis, which leads to accumulation of unfolded proteins in the ER. This activates the unfolded protein response (UPR), an adaptive pathway that aims to clear unfolded proteins and restore ER homeostasis (Hetz 2012). A diversity of NPs has been reported to activate the UPR (Cao et al. 2017).

Both the UPR and the antioxidant response are initially pro-survival pathways induced to regain cellular homeostasis. However, if the insult is too severe or prolonged, the UPR response is switched to a pro-death pathway (Iurlaro and Munoz-Pinedo 2016) and the antioxidant response can no longer protect the cells. Thus, NP-induced stress pathways are two-faced; they may positively contribute to the intended NP-based therapy in certain settings, but may prevent an optimal effect in others. Moreover, excessive stress responses

may give rise to NP cytotoxicity in normal/non-pathological tissues not intended to be affected (Higashisaka et al. 2017). Thus, detailed knowledge on the nature and extent of NP-induced cellular stress responses is required to fully exploit the potential of NPs in therapy and diagnostics.

Poly(alkylcyanoacrylate) (PACA), originally used as surgical glue, is a promising drug carrier material (Vauthier et al. 2003). PACA NPs have the ability to cross the blood-brain barrier (Kreuter 2014), and a PACA-doxorubicin drug formulation is currently in Phase III clinical trials for treatment of advanced hepatocellular carcinoma (ClinicalTrials.gov NCT01655693). Particles are prepared by *in situ* polymerization of alkylcyanoacrylate monomers, and NPs with slightly different chemical compositions can be obtained by using monomers differing only in their alkyl side chains (Morch et al. 2015; Sulheim et al. 2017). Here, we have taken advantage of this to study whether minor alterations in NP composition can affect the type or magnitude of cellular stress responses, and whether this may also affect particle cytotoxicity or even the mode of cell death. We have previously shown that particles synthesized from the monomers butyl-, ethylbutyl-, or octyl cyanoacrylate, termed PBCA, PEBCA, and POCA, respectively, exhibit similar physicochemical characteristics, such as size, polydispersity, and surface charge (Morch et al. 2015; Sulheim et al. 2017). Intriguingly, we here find that the subtle differences in the alkyl side chains of cyanoacrylate dictate both the type and extent of particle-induced stress responses, and determine the mode of cell death induced by the PACA particles. The POCA particles induced ER stress and apoptosis in all cell lines tested, although with slightly different potency. The PBCA particles altered the cellular redox balance and activated a pro-survival integrated stress response downstream of the eIF2α kinase HRI. The PEBCA particles induced redox imbalance during cystine starvation and potently induced an Nrf2-mediated antioxidant response. Importantly, PBCA particles induced ferroptosis, a recently described necrotic cell death pathway that constitutes

a promising druggable cell death pathway in apoptosis-resistant cancer cells, including cancer stem cells (Hangauer et al. 2017; Lu et al. 2017; Stockwell et al. 2017). Thus, the highly similar PACA particles differentially activated cellular stress, and the final outcome of the PACA treatment depended on the cells' ability to mount protective stress responses.

Materials and methods

Materials

ISRIB, propidium iodide (PI), thapsigargin (TG), sodium arsenite (SA), H_2O_2, buthionine sulfoximine (BSO), reduced glutathione (GSH), N-acetyl cysteine (NAC), liproxstatin, ferrostatin, deferiprone (DFP), L-methionine, L-cystine, β-mercaptoethanol, trichloroacetic acid, Kolliphor® HS15 and Pluronic® F68 were all from Sigma. zVAD-fmk was from EMD Millipore Corporation. The PERK inhibitor GSK2606414 was from Calbiochem. Butyl-, ethylbutyl-, and octyl cyanoacrylate were kind gifts from Henkel Biomedical. Miglyol 810N was a kind gift from Cremer. pHTAM was a kind gift from Dr. Andreas Åslund.

Nanoparticle synthesis

PACA NPs were prepared using the mini-emulsion polymerization method as previously described (Sulheim et al. 2017). Briefly, PBCA, PEBCA, or POCA NPs were made by mixing the oil phase, consisting of the monomers butyl-, ethylbutyl-, or octyl cyanoacrylate (2.25 g), a neutral oil (Miglyol 810N, 2 wt%), and the fluorescent dye pentamer hydrogen thiophene acetic acid methyl ester (pHTAM, 0.5 wt%), with the aqueous phase consisting of hydrochloric acid (0.1 M, 25 ml) and the PEG-surfactants Kolliphor® HS15 (6 mM) and Pluronic® F68 (1 mM). The oil in water mini-emulsion was made using a tip sonifier (Branson, 30% amplitude, 6x30 sec with 10 sec pauses, on ice). The polymerization was

carried out at room temperature overnight. The pH was increased to pH 5 using 0.1 M NaOH and the polymerization continued for 5 hours. Surplus of surfactants were removed by extensive dialysis against 1 mM HCl (pH 3). The size, size distribution and ζ-potential were determined using dynamic and electrophoretic light scattering (Zetasizer Nano ZS, Malvern Instruments) in 0.01 M phosphate buffer, pH 7. The reported NP mean diameter (nm) is the *Z*-average.

Cells and treatments

The cell lines MDA-MB-231, Huh7, SW480, HCT116, PC3, and HeLa were obtained from ATCC and maintained in either RPMI or DMEM containing GlutaMAX™ (Sigma-Aldrich) and supplemented with 10% fetal calf serum, 100 U ml^{-1} penicillin, and 100 µg ml^{-1} streptomycin at 37 °C under 5% CO_2. Cell lines were authenticated and regularly tested for mycoplasma contamination. HAP1 WT cells, HAP1 cells that bear only a non-phosphorylatable version of eIF2α (S51A), or HAP1 cells lacking each of the eIF2α kinases - denoted ΔHRI, ΔPERK, ΔGCN2, and ΔPKR - were kind gifts from Dr. Pavel Ivanov (Brigham and Women's Hospital, Boston, USA) (Aulas et al. 2017). The HAP1 cells were maintained in Iscove's Modified Dulbecco's Medium (IMDM, Sigma-Aldrich) with L-glutamine and supplemented with 10% fetal calf serum, 100 U ml^{-1} penicillin, and 100 µg ml^{-1} streptomycin. All cells were seeded one day prior to the experiments. For inhibitor studies, cells were pretreated with the inhibitor at the indicated concentration for 30 minutes before addition of PACA particles. The cellular ATP level (as a surrogate for viability) was measured using the CellTiter-Glo® Luminescent Cell Viability Assay (Promega) and cell death was measured by the CellTox™ Green Cytotoxicity Assay (Promega) according to the manufacturer's procedures. Both luminescence and fluorescence were measured by a Synergy2 plate reader (BioTek). Determination of particle cell-association was performed by

detection of the pHTAM fluorescence of the PACA particles by flow cytometry. Cells were treated with 25 μg ml^{-1} of the three particle types for 2 hours at either 4 °C, which determines cellular binding of the particles, or at 37 °C, which also allows endocytosis of the PACA particles. The cells were thoroughly washed with PBS to remove loosely bound particles. Subsequently, the cells were harvested by Accutase® Cell Detachment Solution (Sigma-Aldrich), pelleted, resuspended in PBS, and subjected to flow cytometry analysis. The dye was excited using a 406 nm (100 mW) solid state diode laser and detected with the 450/50 nm bandpass filter detector on an LSR II Flow Cytometer (BD Bioscience) controlled by the FACSDiva software. Propidium iodide (PI) was used as live-dead stain to aquire at least 10,000 live cells (PI-negative) for each measurement. PI was excited using a 561 nm (45 mW) laser and detected using a 610/20 nm bandpass filter and a 600 nm longpass dichroic filter. Cystine-free medium was prepared by supplementing DMEM without cystine and methionine (#21013, Gibco) with L-methionine (200 μM), 10% fetal calf serum, 4 mM GlutaMAX™ (Gibco), 100 U ml^{-1} penicillin, and 100 μg ml^{-1} streptomycin. Starvation for amino acids was performed in Earle's balanced salt solution (EBSS, Gibco). Determination of protein synthesis was performed by incubating the cells in leucine-free HEPES-buffered medium complemented with 2 μCi ml^{-1} [^{3}H]leucine (PerkinElmer) at 37 °C for 20 min after PBCA-treatment for the indicated times. Then proteins were precipitated with 5% (w/v) trichloroacetic acid and washed once with the same solution. Finally, the proteins were dissolved in 0.1 M KOH and radioactively labeled leucine-incorporation was quantified by β-counting with a Tri-Carb 2100TR® Liquid Scintillation Analyzer (Packard Bioscience).

Immunoblotting

For preparation of total cell lysates, treated cells were washed with cold phosphate buffered saline (PBS) and lysed directly in 1.1x Laemmli sample buffer. The lysate was boiled and

sonicated briefly to reduce viscosity. For the HAP1 cell lines, cells were washed in cold PBS and lysed (0.1 M NaCl, 10 mM Na_2HPO_4, pH 7.4, 1 mM EDTA, 1% Triton X-100, 60 mM n-octyl β-D-glucopyranoside, and a mixture of protease (cOmplete) and phosphatase (PhosSTOP) inhibitors (Roche)). The lysate was sonicated and the protein concentration of the cleared lysate was measured by BCA assay (Thermo Scientific). Equal amounts of protein were loaded on the gel. All lysates were separated by 4-20% SDS-PAGE and transferred to a PVDF membrane. The membrane was blocked by drying followed by overnight incubation with the indicated primary antibodies in 5% BSA, 35 minutes incubation with HRP-conjugated secondary antibodies and detection with SuperSignal West Dura Extended Duration Substrate (Thermo Scientific) in a ChemiDoc Imaging System (Bio-Rad). The signal intensities were quantified by the Quantity One software (Bio-Rad) and were normalized to the loading control. The following antibodies were used: Ubiquitin (#3936), eIF2α (#5324), PERK (#5683), phospho-eIF2α^{Ser51} (p-eIF2α, #3398), ATF4 (#11815), CHOP (#2895), GCN2 (#3302), PARP (#9542), cleaved caspase-3 (#9661), and xCT/SLC7A11 (#12691) all from Cell Signaling Technology, and XBP1s (#619502, BioLegend), PKR (#ab32052, Abcam), and Actin (#CLT9001, Cedarlane).

Mass spectrometry analyses

HCT116 cells were treated with 25 μg ml^{-1} of PBCA, PEBCA or POCA particles and after 4 hours incubation the medium was removed and cells lysed with urea buffer (8 M urea, 2 M thiourea, 50 mM NaCl, 12.5 mM Tris-glycine, and a mixture of protease (cOmplete) and phosphatase (PhosSTOP) inhibitors (Roche)). To include detached cells, the medium was aspirated and centrifuged at 10,000 x g and resulting pellets combined with cell lysates. Crude cell extracts were sonicated and centrifuged to remove cell debris. Cell lysates were digested with trypsin and obtained peptides subjected to LC/MS/MS separation and identification by

an LTQ-Orbitrap XL followed by MaxQuant analysis essentially as described by Hessvik (2016).

Determination of reactive oxygen species (ROS) production

Intracellular ROS production was detected by the chloromethyl derivative of the fluorogenic dye 2',7'-dichlorodihydrofluorescein diacetate (CM-H_2DCFDA, Invitrogen) according to the manufacturer's procedure. Cells (1.5×10^4 cells $well^{-1}$) were pre-incubated with the dye (10 µM, 45 minutes), rinsed and placed in fresh medium without phenol red in the presence or absence of N-acetyl cysteine (NAC, 5 mM). Subsequently, the cells were treated for 30 minutes with PACA particles, or H_2O_2 (100 µM) as a positive control. Fluorescence intensity was measured by a Synergy2 plate reader (BioTek) with excitation and emission wavelengths of 485 nm and 528 nm, respectively.

Glutathione measurement

The intracellular concentration of reduced glutathione (GSH) was determined with o-phthalaldehyde essentially as previously described (Senft et al. 2000). The PACA-treated cells (5×10^5 cells $well^{-1}$) were harvested by Accutase® Cell Detachment Solution (Sigma-Aldrich), washed with PBS, lysed (0.1 M NaCl, 10 mM Na_2HPO_4, pH 7.4, 1 mM EDTA, 1% Triton X-100, 60 mM n-octyl β-D-glucopyranoside, and cOmplete protease inhibitor (Roche)) and precipitated with RQB-TCA solution (20 mM HCl, 5 mM diethylene triamine pentaacetic acid, 10 mM ascorbic acid, 10% trichloroacetic acid) on ice for 30 minutes. Subsequently, the cell lysates were centrifuged (10 minutes, 13,000 rpm) and the supernatants were incubated for 30 minutes at room temperature with 50 µl of phosphate buffer (pH 8.0) containing o-phthalaldehyde in methanol (5 mg/ml). The fluorescence intensity of the formed complex was measured by a Synergy2 plate reader (BioTek) with excitation and emission wavelengths of 360 nm and 460 nm, respectively. Inhibition of glutathione synthesis by BSO (100 µM, 18

hours) was used as a positive control for GSH depletion. The GSH content was normalized to the protein content of each lysate, as determined by the BCA assay (Thermo Scientific).

Lipid peroxidation detection

Lipid peroxidation was measured using the dye C11-BODIPY (581/591, Thermo Fisher Scientific). Cells treated with PACA NPs for 4 hours were labeled with C11-BODIPY (2.5 μM, 30 minutes). Subsequently, the stained cells were harvested by Accutase® Cell Detachment Solution (Sigma-Aldrich), pelleted, resuspended in PBS and subjected to flow cytometry analysis. The dye was excited using a 488 nm Ar laser and detected with the FL1 (545 nm) detector on an LSR II Flow Cytometer (BD Bioscience). At least 10,000 cells were acquired for each measurement.

Quantitative real-time RT-PCR

Total RNA was isolated from cells using the RNeasy Plus Mini Kit (QIAGEN), according to the manufacturer's procedure. 0.8 μg of total RNA was used for cDNA synthesis using the iScript cDNA Synthesis kit (Bio-Rad Laboratories). The real-time PCR analysis was run on a LightCycler 480 Real-Time PCR System using LightCycler 480 SYBR green 1 Master mix (Roche). The cycling conditions were 95 °C for 5 minutes, followed by 45 cycles of 95 °C 10 sec, 60 °C 20 sec, and 72 °C 10 sec. The house-keeping gene TBP (TATA box binding protein) served as an internal control and LightCycler 480 Relative Quantification Software (Roche) was used for quantification. The following QuantiTect®Primer Assays were used: Hs_EIF2AK4 (QT01036350), Hs_EIF2AK3 (QT00066003), Hs_EIF2AK2 (QT00022960), Hs_EIF2AK1 (QT01018920), Hs_ATF4 (QT00074466), Hs_TBP (QT00000721), Hs_SLC7A11 (QT00002674), Hs_GCLM (QT00038710), Hs_FTH1 (QT00072681), and Hs_HMOX (QT00092645).

Transfection of cells with siRNAs

Small interfering RNAs (siRNAs) were introduced into MDA-MB-231 cells by reverse transfection. The siRNAs were diluted in RPMI and mixed with Lipofectamine RNAiMax (Invitrogen) before addition to 3 x 10^5 freshly trypsinized cells in 6-well culture plates at a final siRNA-concentration of 10 nM. The culture medium was exchanged the next day. The experimental treatments were initiated 48 hours after transfection. The following siRNAs were used (Silencer Select siRNAs from Ambion): Silencer® Select Negative Control #1 (4390843), siPERK-1 (ID 18103), siPERK-2 (ID 18101), siATF4-1 (ID 1702), siATF4-2 (ID 1704), siHRI-1 (ID 25822), siHRI-2 (ID 25823), siNrf2-1 (ID 9492), siNrf2-2 (ID 9493), siSLC7A11-1 (ID 24289), siSLC7A11-2 (ID 24291), siPKR-1 (ID 11185), siPKR-2 (ID 11186), or ON-TARGETplus Non-targeting siRNA #1(D-001810-01-05), ON-TARGET plus siGCN2-1 (J-005314-07-0010) and siGCN2-2 (J-005314-06-0010) from Dharmacon. In the quadruple knockdown of ISR kinases 10 nM of each of the following siRNAs were included: siPERK-1, siGCN2-2, siPKR-1, siHRI-1. This was compared to 40 nM of negative control siRNA. In the double knockdown of ATF4 and Nrf2, 10 nM of each siRNA (siATF4-1 and siNrf2-2) was mixed and compared to 20 nM of negative control siRNA.

Microscopy

Phase contrast images were acquired by an Eclipse TS100 microscope (Nikon) equipped with a 20x objective and a Digital Sight camera (Nikon). Cell death was visualized by the fluorogenic dye CellTox™ Green Cytotoxicity reagent (Promega) after 24 hours treatment of the cells with PACA particles. Merged fluorescent and phase contrast wide-field images were acquired by the EVOS FL Cell Imaging System (Thermo Fisher Scientific).

For live cell microscopy cells seeded on glass bottom dishes (MatTek) were imaged on a Deltavision microscope (Applied Precision) equipped with Elite TruLight Illumination

System, a CoolSNAP HQ2 camera, and a 60× Plan-Apochromat (1.42 NA) objective. The microscope stage was kept at 37 °C under 5% CO_2 by an incubation chamber. For detection of caspase-3/7 activity and cell death, cells grown in 4-chamber MatTek dishes were treated with PACA particles in the presence of the fluorogenic dye CellEvent™ Caspase 3/7 Green Detection Reagent (Invitrogen) and propidium iodide (2 μg ml^{-1}). Time-lapse images (5 z-sections 2.5 μm apart) were acquired every 10 minutes for up to 24 hours. The images were deconvolved and z-projected using the softWoRx software (Applied Precision).

Statistical analysis

Mean values ± standard error of the mean (SEM) were calculated for each condition. The statistical significance of the differences was determined by two-tailed unpaired Student's t-test, with equal or unequal variances, as appropriate; *, $p<0.05$; **, $p<0.01$; ***, $p<0.001$.

Results

Different PACA particles exert differential cytotoxicity and induction of heat shock proteins

PACA particles with only minor differences in their cyanoacrylate side chains (Figure 1B) were produced by *in situ* polymerization of the alkylcyanoacrylate monomers butyl- (PBCA), ethylbutyl- (PEBCA), or octyl cyanoacrylate (POCA) as previously described (Morch et al. 2015; Sulheim et al. 2017). The resulting particles exhibited similar mean sizes, in the range of 133-153 nm, with a relatively narrow size distribution. All three NPs were slightly negatively charged with a zeta-potential of approximately -3 mV (Figure 1B). The size of the PACA particles was found to be stable upon incubation in complete growth medium with 10% fetal calf serum over 24 hours (data not shown). When particle cytotoxicity was compared by adding the particles at increasing concentrations to a panel of cancer cell lines

(MDA-MB-231, Huh7, SW480, HCT116, PC3, and HeLa) a striking difference in particle cytotoxicity was observed between the three types of particles. The POCA particles consistently exerted the highest cytotoxicity, whereas PEBCA particles were the least toxic (Figure 1C). This is in agreement with our previous screening study of 12 cancer cell lines (Sulheim et al. 2017). We also observed differences in PACA cytotoxicity between the cell lines. HCT116 and HeLa cells seemed to be less sensitive to POCA particles than the other cell types, whereas the cytotoxicity of PEBCA and PBCA particles showed less variation across the panel of cells (Figure 1C). Importantly, the differences in cytotoxicity, both between particle types and between cell lines, could not be explained by differences in particle uptake, since we only observed minor variations in particle binding and uptake (Supplementary Figure 1) (Sulheim et al. 2016; Sulheim et al. 2017).

To assess whether the differences in PACA cytotoxicity between the particle types is caused by particle-specific induction of cellular stress responses, we first tested whether the PACA particles would induce accumulation of ubiquitinated proteins, a hallmark of altered cellular homeostasis (Hetz 2012). When cells were treated with 25 $\mu g\ ml^{-1}$ (an intermediary concentration with respect to cytotoxicity at 24 hours) of each variant of PACA NPs, a buildup of ubiquitinated proteins was observed within the first 4 hours of treatment in all cell lines tested, although to a variable degree, and with all three PACAs (Figure 1D). By mass spectrometry analyses we also observed that the particles induced increased expression of a wide variety of heat shock family proteins, a common response to cellular stress and accumulation of misfolded proteins (Figure 1E). Overall, the PBCA and POCA particles exerted the most potent effects on both accumulation of ubiquitinated proteins and induction of heat shock family proteins.

The PACA particles differentially induce the unfolded protein response

Accumulation of ubiquitinated proteins may result from ubiquitination of cytosolic proteins or an overwhelming translocation of unfolded or misfolded proteins from the ER to the cytosol. The latter case would be expected to result from decreased ER protein folding capacity (termed ER stress), which activates the UPR. To assess whether the PACA particles activate the UPR, we used the PERK pathway as readout (Figure 2A) and the ER stressor thapsigargin (Thastrup et al. 1990) as a positive control (Supplementary Figure 2A). Accumulation of unfolded or misfolded proteins in the ER lumen activates PERK, which leads to phosphorylation, and thus inactivation, of eIF2α and subsequent shut down of global protein synthesis (Hetz 2012). Phosphorylation of eIF2α leads to selective induction of translation of the transcription factor ATF4, which initiates transcription of genes encoding ER chaperones, amino acid transporters, and antioxidant proteins that contribute to restoration of cellular homeostasis (Hetz 2012). ATF4 can also increase the expression of the transcription factor CHOP. Intriguingly, the three variants of PACA NPs induced a highly different UPR activation pattern. The POCA particles induced the most prominent PERK activation recognized by an upward shift in PERK migration, already at 2-4 hours and at concentrations as low as 12.5 μg ml^{-1} (Figure 2B, Supplementary Figure 2A, B). The PERK bandshift, induced by both thapsigargin and POCA particles, was totally blocked by the PERK inhibitor GSK2606414, demonstrating the specificity of the bandshift as a readout for PERK activation (Supplementary Figure 2A). We noted that higher concentrations of POCA (25 μg ml^{-1}) were required for PERK activation in HCT116 and HeLa cells (Supplementary Figure 2B). The POCA particles also induced downstream phosphorylation of eIF2α and accumulation of ATF4 and CHOP (Figure 2B, Supplementary Figure 2B). Notably, in certain cell lines a clear detection of ATF4 accumulation was challenging due to the presence of a closely migrating band (indicated by an asterisk in the figures). This band was identified as being unspecific,

since it was unchanged upon siRNA-mediated depletion of ATF4 (Supplementary Figure 2C, D). The PEBCA particles induced a weaker PERK pathway activation that could generally only be discerned at elevated concentrations (50 μg ml^{-1}) (Figure 2B, Supplementary Figure 2B). Surprisingly, 25 μg ml^{-1} of PBCA particles induced a rapid and potent phosphorylation of eIF2α and accumulation of ATF4 without a clear upstream PERK activation (Figure 2B), and a less marked shift than observed with PEBCA and POCA at elevated concentrations (Supplementary Figure 2B). This might suggest that eIF2α is predominantly phosphorylated by an alternative kinase in PBCA-treated cells, and thus, that the stress is of a different nature.

To assess whether the PACA particles activate the IRE1 ER stress pathway, we probed for the IRE1 downstream target XBP1s (Hetz 2012) (Figure 2A). Accumulation of XBP1s was detected after treatment with low concentrations of POCA. The required concentration varied between the cell lines. PEBCA and PBCA particles also increased XBP1s levels, but this only occurred at the highest concentrations tested (Supplementary Figure 2B). Together, this suggests that ER stress is differently activated by the highly similar particles; it is potently induced by POCA particles, only activated by high PEBCA concentrations, and induced to a low extent by PBCA particles.

PBCA-induced integrated stress response activation is mediated by HRI

Phosphorylation of eIF2α can not only be observed as a response to ER stress and PERK activation, but also upon activation of three other eIF2α kinases, GCN2, PKR or HRI, through the so-called *integrated stress response* (ISR) (Figure 2A). These kinases sense various internal or external stressors, including amino acid starvation, viral infection, oxidative stress, proteasomal inhibition, and ER stress (Pakos-Zebrucka et al. 2016). In order to assess whether the PBCA-induced ATF4 accumulation was mediated by the ISR, we employed the recently developed ISR inhibitor ISRIB, which blocks all downstream effects of phosphorylated eIF2α

(Sidrauski et al. 2013) (Figure 2A). For these studies we chose the MDA-MB-231 cells, as they displayed a rapid and potent phosphorylation of eIF2α and a clear accumulation of ATF4 (Figure 2B). Indeed, the PBCA-induced accumulation of ATF4 was inhibited by ISRIB (Figure 2C, D). Moreover, there was a good correlation between PBCA-induced phosphorylation of eIF2α and reduction in global protein synthesis (Figure 2D, E), and the reduction of protein synthesis was partially reversed by ISRIB (Figure 2E). Thus, the ISR seems to be activated as an acute response to PBCA particles. In an attempt to identify the eIF2α kinase(s) responsible for this activation, the four ISR kinases were depleted by siRNA. In line with the ISRIB data, simultaneous depletion of all kinases (Supplementary Figure 3A, B) strongly reduced PBCA-induced phosphorylation of eIF2α and accumulation of ATF4 (Supplementary Figure 3C-E). Individual knockdown of PERK, GCN2 or PKR did not prevent the phosphorylation of eIF2α, whereas knockdown of HRI slightly reduced PBCA-induced p-eIF2α levels (Figure 2F). This may suggest that HRI is involved in the PBCA-induced stress response. To further assess the involvement of the individual eIF2α kinases, we took advantage of HAP1 cells with CRISPR/Cas9-mediated knockout of each eIF2α kinase (Aulas et al. 2017) (Supplementary Figure 3F). As a demonstration of the functional knockout and the stress-specificity of these kinases, we observed that the phosphorylation of eIF2α was selectively abolished in ΔGCN2 cells starved for amino acids in EBSS, in ΔHRI cells treated with sodium arsenite, the selective activator of HRI (Lu et al. 2001), and in ΔPERK cells treated with thapsigargin (Supplementary Figure 3G) (Aulas et al. 2017). When these cells were treated with PBCA particles, the phosphorylation of eIF2α was rapidly induced in WT cells, but importantly the phosphorylation was equally potent in ΔPERK, ΔGCN2, or ΔPKR cells (Figure 2G, H, quantified at the 1 hour time point), strengthening the notion that these kinases are not singly responsible for the PBCA-induced stress response. In contrast, phosphorylation of eIF2α was significantly reduced in ΔHRI cells (Figure 2G, H). Also when

using protein synthesis reduction as a readout for ISR activation, PBCA-induced activation of HRI was suggested (Supplementary Figure 3H). Notably, as in MDA-MB-231 cells, the PBCA-induced inhibition of protein synthesis was not solely mediated by the ISR, as revealed by reduction of protein synthesis also in cells expressing the S51A unphosphorylatable eIF2α that is insensitive to ISR activation. Thus, when taking the level of protein synthesis in S51A cells into account, the ΔHRI cells were much less sensitive to ISR-dependent PBCA-induced inhibition of protein synthesis than WT cells (Supplementary Figure 3H), resembling data from treatment with sodium arsenite. In contrast to the selective involvement of HRI in PBCA-induced stress, phosphorylation of eIF2α upon treatment with PEBCA or POCA particles seemed to require several eIF2α kinases. Although there was a slight decrease in ΔHRI cells, knockout of each kinase alone did not significantly prevent particle-induced p-eIF2α (Supplementary Figure 3I, J). In conclusion, whereas ER stress is strongly induced by POCA and weakly by PEBCA and PBCA, all PACA particles, including POCA, induce the ISR, in a manner that relies on multiple ISR kinases, but with a particular dependency on HRI in PBCA-treated cells.

POCA particles selectively induce apoptotic cell death

Intrigued by the differential effects of the PACA particles on cytotoxicity and cellular stress, we aimed to identify the mode of cell death induced by the three PACA variants. The panel of cell lines was treated for 24 hours with particle concentrations found to be cytotoxic by the ATP assay (Figure 1C). In all cell lines the POCA particles induced apoptotic phenotypes, such as extensive plasma membrane blebbing and cell shrinkage (Supplementary Figure 4, arrows). In contrast, treatment with PEBCA and PBCA particles mostly led to cell rounding or detachment, cell swelling or rupture, whereas phenotypes associated with apoptosis were only occasionally observed. Apoptosis induction was further assessed by immunoblotting for

well-known apoptosis markers such as cleavage of caspase-3 and the caspase-3/7 substrate PARP. Detached cells were spun down and included in the lysates. Strikingly, the POCA particles induced cleavage of caspase-3 and PARP at concentrations as low as 12.5 or 25 μg ml^{-1} (Figure 3A), and already after 8 hours of treatment (Supplementary Figure 5). In line with the reduced cytotoxicity of POCA particles in HCT116 and HeLa cells, caspase activation required higher particle concentrations in these cells. In contrast to POCA particles, PEBCA and PBCA particles generally promoted less cleavage of caspase-3 or PARP, and only at high particle concentrations (Figure 3A). To further visualize the particle-selective cell death modes, we turned to live cell imaging. In particle-treated Huh7 and MDA-MB-231 cells, apoptosis induction was detected by the fluorogenic CellEvent™ caspase 3/7 substrate, and cell death was identified by the nuclear dye propidium iodide (PI), which selectively stains cells with compromised plasma membrane integrity. In POCA-treated cells the green caspase 3/7 stain preceded the red PI-staining in both cell types, indicating that apoptosis is induced before the final cell rupture (Figure 3B, Supplementary videos 1-6). In contrast, when cells were treated with PEBCA or PBCA particles the nuclei acquired PI-staining in the absence of caspase activation (Figure 3B, Supplementary videos 1-6), indicating that these particles mainly induce a necrotic type of cell death. A selective induction of apoptosis by POCA particles was also demonstrated by the protective effect of the pan-caspase inhibitor z-VAD in MDA-MB-231 cells (Figure 3C).

PBCA particles induce ferroptosis in MDA-MB-231 cells

We next asked what type of non-apoptotic cell death may be induced by PEBCA and PBCA. In recent years, the term necrosis has been subdivided into a plethora of differentially regulated necrotic cell death pathways (Conrad et al. 2016). A recently discovered subtype of regulated necrosis, called ferroptosis, is associated with accumulation of ROS in an iron-

dependent manner, loss of GSH, and excessive lipid peroxidation (Lu et al. 2017; Stockwell et al. 2017) (Figure 4A). It was recently demonstrated that some of the most drug-resistant and hard-to-kill cancer cells, namely those that have undergone epithelial-to-mesenchymal transition (Viswanathan et al. 2017) and those that persist after conventional chemotherapy, often referred to as cancer stem cells (Hangauer et al. 2017), are highly sensitive to ferroptosis. Ferroptosis-sensitive cells are characterized by decreased levels of GSH and NADPH (Hangauer et al. 2017), are highly vulnerable to GSH depletion, and depend on constant import of the GSH precursor cystine via the cystine-glutamate antiporter xCT/SLC7A11 (Lu et al. 2017). MDA-MB-231 is a representative cell line for ferroptosis studies as it is highly mesenchymal, with cancer stem cell-like properties (Morata-Tarifa et al. 2016). As PEBCA particles exerted low cytotoxicity in these cells (Figure 1C), we initially focused on PBCA-induced cell death. Cell death was assessed by the CellTox™ Green cytotoxicity assay, in which only cells with loss of plasma membrane integrity are stained. Strikingly, PBCA cytotoxicity was almost totally reversed by the ferroptosis inhibitors ferrostatin and liproxstatin, which are lipophilic, small-molecule antioxidants (Zilka et al. 2017) (Figure 4B, C). Also the iron chelator deferiprone (DFP) abolished PBCA cytotoxicity, further implicating ferroptosis, whereas the pan-caspase inhibitor z-VAD had no significant effect.

Ferroptosis is characterized by ROS imbalance, and since PBCA particles activated the ISR downstream of the ROS-sensitive HRI already after 15-30 minutes, we decided to measure early accumulation of cellular ROS by using the probe CM-H_2DCFDA and subjecting the cells to 30 minutes of particle exposure. The ROS levels were moderately, but significantly increased by both PEBCA and PBCA, whereas only a slight increase, that did not reach statistical significance, was observed with POCA (Figure 4D). Ferroptosis is also characterized by depletion of the main cellular antioxidant, GSH. Indeed, the intracellular

GSH level, as determined by o-phthalaldehyde, was partially depleted upon treatment with PBCA (Figure 4E). Thus, PBCA clearly induced redox imbalance. Importantly, this seemed to trigger the downstream stress responses, as treatment with excess GSH completely abolished PBCA-induced accumulation of ubiquitinated proteins, phosphorylation of eIF2α, and accumulation of ATF4 (Figure 4F, quantifications in Supplementary Figure 6A-C). Also the cytotoxicity of PBCA particles was fully reversed by either excess GSH or NAC, a precursor of GSH (van Zandwijk 1995) (Figure 4G). In contrast, POCA cytotoxicity was not prevented by antioxidant treatment (Figure 4G), pointing to a fundamental difference in the stress induction and cytotoxic action of these particles. As ferroptosis is characterized by lipid peroxidation, we measured the extent of peroxidated lipids by employing the probe BODIPY-C11. Indeed, treatment with PBCA particles induced lipid peroxidation in a liproxstatin-sensitive manner (Figure 4H).

Both PEBCA and PBCA particles promote ferroptosis under cystine-starvation conditions

The cellular import of cystine via xCT/SLC7A11 has been identified as one of the key regulators of ferroptosis (Stockwell et al. 2017) (Figure 5A). Imported cystine is converted to *cysteine*, which is the rate-limiting substrate in GSH synthesis. Cystine availability is thus an important determinant of cellular redox capacity. We asked whether cystine availability affects PBCA cytotoxicity. Strikingly, when MDA-MB-231 cells were incubated in medium lacking cystine, potent cell death was induced already with 12.5 μg ml^{-1} PBCA, a concentration that does not induce cytotoxicity in full medium (Figure 5B, C). This cell death was fully inhibited by the ferroptosis inhibitors ferrostatin, liproxstatin, or DFP, or by re-addition of cystine, whereas z-VAD had no effect (Figure 5B, C). Surprisingly, in cystine-free medium even the relatively non-cytotoxic PEBCA particles exerted potent ferroptosis-dependent cytotoxicity at 12.5 μg ml^{-1} (Figure 5B, C). To test whether the increased

vulnerability towards these two PACA particles was caused by a lower antioxidant capacity in cystine-starved cells, the cellular GSH levels were measured. Indeed, four hours of cystine starvation was sufficient to slightly reduce the level of GSH (Figure 5D), and under these conditions treatment with 12.5 μg ml^{-1} of PEBCA or PBCA particles strongly reduced the GSH levels (Figure 5D). Concomitant with reduction of GSH, low concentrations of PEBCA and PBCA (6.25 and 12.5 μg ml^{-1}) significantly induced lipid ROS generation in cells starved for cystine (Figure 5E). Taken together, the ability of PBCA to induce ferroptosis is strongly increased upon reduction of cystine availability, and under cystine-free conditions also the PEBCA particles induce GSH depletion, lipid ROS generation and ferroptosis.

PEBCA- and PBCA-induced accumulation of ATF4 and Nrf2 counteracts ferroptosis in MDA-MB-231 cells

As treatment with PBCA particles potently induced accumulation of ATF4 in a GSH-dependent manner (Figure 4F), and ATF4 mediates transcription of antioxidant proteins, we asked whether ATF4 contributes to cell viability in PBCA-treated cells. Indeed, siRNA-mediated depletion of ATF4 in MDA-MB-231 cells further potentiated PBCA cytotoxicity at low particle concentrations (up to 25 μg ml^{-1}) (Figure 5F, Supplementary Figure 7A), indicating that ATF4 accumulation acts as a pro-survival response. ATF4 is not only regulated by increased translation, but also at the transcriptional level. In line with this, *ATF4* mRNA was induced by low PBCA concentrations, reaching maximum levels at 12.5 μg ml^{-1} of PBCA (Figure 5G). In accordance with the lower cytotoxicity of PEBCA particles, *ATF4* transcription was maximally induced at higher PEBCA concentrations (50 μg ml^{-1}) (Figure 5G). Furthermore, the importance of cystine availability in PBCA/PEBCA-induced stress responses was demonstrated by the significantly higher levels of ATF4 induced under cystine starvation conditions even at low particle concentrations (Figure 5H, I). Importantly, both PEBCA and PBCA particles induced ATF4-dependent transcription of *SLC7A11* (Figure 5J).

As PEBCA and PBCA particles exert comparable cytotoxicity upon cystine starvation (Figure 5C), whereas the particle cytotoxicity is highly different in complete cell medium (Figure 1C), the question remains whether the PEBCA particles have the ability to activate additional cytoprotective pathways. Nrf2 is a master transcriptional activator of cytoprotective genes in response to electrophiles and oxidants (Itoh et al. 1997). Normally, Nrf2 levels are kept low by ubiquitination via the E3 ubiquitin ligase adaptor Keap1, but the presence of cytotoxic substances blocks the interaction with Keap1 and thus prevents Nrf2 degradation (Bellezza et al. 2018). Interestingly, four hours of treatment with PEBCA particles increased Nrf2 protein levels more potently than PBCA particles. The maximum PBCA-induced Nrf2 accumulation was reached already at 25 $\mu g\ ml^{-1}$ and then decreased at higher concentrations, whereas Nrf2 was accumulated in a dose-dependent manner and to a stronger extent by PEBCA particles (Figure 6A), resembling the transcriptional activation of *ATF4* with respect to the dose-response relationship (Figure 5G). Similarly, when the incubation was prolonged to 8 hours, the levels of Nrf2 remained strongly elevated in cells treated with high concentrations of PEBCA particles (Figure 6A). Also at 16 hours there was a faint band of Nrf2 at 50 $\mu g\ ml^{-1}$ of PEBCA.

To investigate whether this prolonged accumulation of Nrf2 contributes to the difference in particle cytotoxicity, Nrf2 was depleted by siRNA (Figure 6B). Knockdown of Nrf2 rendered cells highly sensitive to both PEBCA and PBCA particles (Figure 6C), but importantly, the sensitization induced by Nrf2 depletion was significantly higher in PEBCA-treated cells (Supplementary Figure 7B). Thus, it seems that the increased ability to activate a prolonged cell protective response contributes to the lower cytotoxicity of PEBCA particles. Furthermore, in Nrf2-depleted cells low concentrations of PEBCA and PBCA particles, which were non-cytotoxic in control transfected cells, potently increased cell death in a manner fully reversible by the ferroptosis inhibitors ferrostatin, liproxstatin and DFP, but not z-VAD,

implicating induction of ferroptotic cell death upon Nrf2-depletion (Figure 6D, E). This demonstrates that Nrf2 protects the cells against particle-induced ferroptosis. Combined depletion of Nrf2 and ATF4 dramatically sensitized the cells towards both PEBCA and PBCA particles (Supplementary Figure 7C). Notably, Nrf2 has been shown to induce *ATF4* transcription during oxidative stress (Afonyushkin et al. 2010; Miyamoto et al. 2011). In line with the significant accumulation of Nrf2, PEBCA particles induced *ATF4* transcription in an Nrf2-dependent manner (Supplementary Figure 7D), in this way connecting these stress pathways.

Several of the transcriptional targets of Nrf2 are relevant in protection against ferroptosis, such as heme oxygenase 1 (*HMOX1*), ferritin heavy chain (*FTH1*) involved in iron storage, the cystine transporter (*SLC7A11*), or the rate-limiting enzyme in the GSH biosynthesis pathway, glutamate-cysteine ligase (*GCLM*) (Bellezza et al. 2018; Stockwell et al. 2017). Transcription of several of these targets was induced by both PEBCA and PBCA in an Nrf2-dependent manner (Figure 6F, Supplementary Figure 7E), and again the PEBCA particles exerted a more potent effect, which was reflected by a higher expression of SLC7A11 also on the protein level (Supplementary Figure 7F). To directly explore the significance of the cystine transporter in PBCA/PEBCA-cytotoxicity, MDA-MB-231 cells were depleted for SLC7A11 by siRNA (Figure 6G). This strongly sensitized the cells towards PEBCA and PBCA particles (Figure 6H), in a manner similar to double knockdown of Nrf2 and ATF4 (Supplementary Figure 7B). In cells depleted for SLC7A11, low concentrations of PBCA/PEBCA particles potently induced cell death, in a manner fully reversed by ferroptosis inhibitors, but not z-VAD (Figure 6I, J). To confirm the importance of cystine under these conditions, the cells were treated with β-mercaptoethanol, which reduces extracellular cystine to cysteine that can be imported through the LAT1 transporter (Figure 6K), thus circumventing the need for the xCT/SLC7A11 transporter. Treatment with β-mercaptoethanol

fully reversed the PBCA/PEBCA-induced cell death (Figure 6I, J). Taken together, PEBCA and PBCA particles alter the redox balance, and compensatory cellular stress responses are induced via activation of ATF4 (mainly by PBCA) and Nrf2 (mainly by PEBCA) to regain homeostasis and prevent cell death.

Discussion

Here we have demonstrated that subtle differences in NP structure have significant impact on particle-induced cellular stress responses and the mode of cell death in cancer cells. This highlights the importance of rigorous testing of cellular responses of NP-cell interactions.

The three highly similar PACA particles tested in the current study induced surprisingly variable cellular stress responses and cytotoxicity. From our data, it seems unlikely that the three particles merely affect cells via the same mechanism with different potency. Rather, it seems that each particle induces specific effects during the NP-cell interaction. Moreover, the net effect on cell viability of each particle seems to be determined by the balance between particle-induced pro-death and pro-survival responses (see model in Supplementary Figure 8). For instance both the POCA particles and high concentrations of PEBCA particles clearly induced ER stress, as revealed by activation of PERK, ATF4, CHOP and XBP1s, and yet the particle-induced cytotoxicity was different. Although treatment with both PEBCA and POCA particles affect ER homeostasis, the POCA particles may exert a more acute and severe effect, which renders the cells less able to activate pro-survival pathways to restore homeostasis, and as a result, apoptosis is rapidly induced. The PBCA particles only marginally induced PERK activation, but still induced rapid and potent phosphorylation of eIF2α, which was found to be partially mediated by HRI, the heme-regulated eIF2α kinase (Pakos-Zebrucka et al. 2016). This is, to the best of our knowledge, the first demonstration of activation of HRI in response to NP treatment. HRI responds to

various stressful conditions including heme deficiency, heat shock, proteasomal inhibition, or oxidative stress (Lu et al. 2001; Pakos-Zebrucka et al. 2016). It seems likely that HRI is activated by PBCA through oxidative stress, as the PBCA-induced ISR activation was abolished by GSH and NAC, and since PBCA both induces ROS and depletes cells of GSH.

The accumulated ATF4 seemed to exert a weak pro-survival role at low PBCA concentrations. This is likely caused by the increased ATF4-mediated transcription of components involved in antioxidant responses, such as the cystine transporter xCT/SLC7A11. Furthermore, the PBCA-induced ISR could potentially contribute to cell survival by downregulation of protein synthesis via phosphorylation of eIF2α. Inhibition of protein synthesis could potentially increase the availability of cysteine for GSH production and reduce the amount of misfolded proteins. Cysteine availability for GSH production may also depend on the extent of amino acid liberation through protein degradation pathways, such as proteasomal degradation. Along these lines, inhibition of proteasomal degradation by bortezomib, a promising anti-cancer drug, induced cell death via limiting the levels of intracellular cystine, and thus GSH, in myeloma cells (Starheim et al. 2016). Interestingly, in bortezomib-treated pancreatic cancer cells HRI was recently shown to exert a pro-survival role by downregulating protein synthesis (White et al. 2018).

Our data point to alterations in cellular redox capacity as a key mechanism in both PBCA and PEBCA cytotoxicity. The difference in cytotoxicity between these particles is likely caused by the stronger and more prolonged Nrf2-mediated antioxidant response induced by PEBCA. Both ATF4 and Nrf2 likely contribute to transcription of *SLC7A11*, as depletion of SLC7A11 induced comparable cell death to double knockdown of ATF4 and Nrf2. Increased expression of SLC7A11 is associated with drug resistance and poor survival in several cancer types (Lo et al. 2008), and a subset of triple-negative breast tumors and cell lines, including MDA-MB-231, require expression of SLC7A11 for growth (Timmerman et

al. 2013). In accordance with this, we observed an inverse correlation between cystine availability and PBCA/PEBCA cytotoxicity in MDA-MB-231 cells. Cystine starvation reduced cellular GSH levels, increased lipid peroxidation, and potentiated the cytotoxicity of both PBCA and PEBCA particles. It is unlikely that PBCA cytotoxicity is solely caused by inhibition of cystine import, as cystine starvation alone was much less cytotoxic than treatment with PBCA particles. An alternative scenario is that the particles induce concomitant GSH depletion *and* reduced cystine availability, as shown to be required for ferroptosis induction in HepG2 cells (Yu and Long 2016).

In addition to differences in cytotoxicity between the particle types, we also observed differences between the cell lines. The six cell lines could be roughly divided into two groups; cells with a large difference in PACA cytotoxicity between the three particle types (MDA-MB-231, Huh7, SW480 and PC3) and cells with a more similar cytotoxicity pattern (HCT116 and HeLa). On closer inspection, this pattern seemed to stem from a shift towards lower POCA cytotoxicity for HCT116 and HeLa cells. These cell lines also displayed the lowest PERK activation and caspase activity upon POCA treatment. Combined with our finding that POCA particles are less able to induce protective antioxidant responses than PEBCA and PBCA particles in MDA-MB-231 cells, the possibility exists that the cell type-dependent variation in susceptibility towards POCA-induced cellular stress reflects cell-inherent differences in basal levels of cell protective pathways and detoxification capacity. Thus, HCT116 and HeLa cells may have a higher inherent detoxification capacity that prevents or delays POCA-induced activation of ER stress and apoptosis. Moreover, if our findings from MDA-MB-231 cells represent a general phenomenon, it is tempting to speculate that PEBCA- and PBCA-induced activation of cell protective pathways also explain why Huh7, SW480 and PC3 cells are more resistant to these particles compared to POCA. Such a particle-induced activation would mask cell-inherent differences in basal detoxification ability. Thus, our data

not only illustrates the importance of testing NP cytotoxicity across a broad range of cell types before drawing general conclusions, but also the importance of selecting relevant cell models when assessing tissue-specific or organ-specific NP cytotoxicity. Since accumulation of ROS is a key feature in NP cytotoxicity (Abdal Dayem et al. 2017), selecting cell lines with various levels of basal antioxidant protection would be particularly relevant. Testing NP cytotoxicity solely in cancer cells with strongly elevated antioxidant protection could preclude the detection of potential nanotoxicity. Among other factors, detoxification capacity seems to depend on the type of cellular carbon metabolism (Gentric et al. 2017). Cells relying predominantly on oxidative phosphorylation show higher antioxidant response or detoxification capacity than cells depending on glycolysis. Our data also show the importance of including several assays when assessing nanotoxicity, as cell viability assays alone may not reveal NP-mediated cellular stress responses. Sub-toxic cellular stress responses, particularly prolonged stress, can compromise cell function and may render exposed cells and tissues more vulnerable to additional insults.

Intriguingly, when the redox capacity of MDA-MB-231 cells was reduced by PBCA particles, apoptotic cell death was not induced, but rather the redox-mediated, iron-dependent cell death mechanism known as ferroptosis. Also the PEBCA particles induced ferroptosis when cystine availability was reduced. These findings are of great interest in drug-delivery, as cellular stress that is induced as a response to the nanocarrier itself may be beneficial if these stress responses sensitize the target cells. Many cancer types are particularly sensitive to ferroptosis (Viswanathan et al. 2017; Yu et al. 2017). It was recently demonstrated that inhibition of glutathione peroxidase 4, which is responsible for reduction of peroxidated lipids, leads to ferroptotic cell death of drug-tolerant cancer stem cells in a wide range of cancers (Hangauer et al. 2017). Thus, ferroptosis-inducing compounds have emerged as a promising novel treatment option for multidrug-resistant cancer stem cells. Ferroptosis-

inducing drugs have also shown synergistic effects with chemotherapeutics such as cisplatin (Sato et al. 2018), and doxorubicin (Narang et al. 2007). PEBCA particles loaded with doxorubicin are currently in clinical trials for hepatocellular carcinoma (ClinicalTrials.gov NCT01655693), and since PACA particles accumulate in the liver (Snipstad et al. 2017), they may influence the redox status of the tumor cells and contribute to cell killing by ferroptosis. Our data also suggests that exchanging the PEBCA monomer with PBCA could potentially prove even more efficient in cell killing of drug-resistant cancers. Moreover, induction of a necrotic type of tumor cell death, such as ferroptosis, could potentially contribute to higher tumor infiltration of immune cells, further contributing to tumor clearance (Sarhan et al. 2018). Thus, identification of ferroptosis-inducing NPs is of considerable interest.

How do NPs induce cellular stress responses, and why do the PACAs studied here have different effects? It has been proposed that physical interactions between NPs and the plasma membrane may signal membrane stress to the cell interior (Mouritsen 2011). The interaction between NPs and cellular membranes may lead to alterations in membrane fluidity, the composition of micro-domains, or membrane curvature (Nel et al. 2009). Such membrane alterations are known to affect the activity of membrane proteins like receptors, enzymes, ion channels, and nutrient transporters (Mouritsen 2011). There are no gross differences in physical characteristics of the three PACA particles. They are of similar size, shape and surface charge. However, their alkyl side chains have increasing hydrophobicity in the order PBCA < PEBCA < POCA. Although the particles are PEGylated, the side chain hydrophobicity may dictate the exact composition of the protein corona that are known to surround NPs incubated in biological fluids or complete cell medium containing serum (Barbero et al. 2017). It was recently shown that the hydrophilicity of the NP polymer shell dictated the composition of the protein corona generated in blood (Simon et al. 2018). Although the total amount of adhered protein was equal, the protein pattern was different.

This determined the NP-cell interactions and the nanocarrier's stealth properties. Thus, the different cellular effects of PACA particles may be caused by even minor changes in the protein corona surrounding each particle type. The cell-associated POCA fluorescence was slightly higher than PEBCA and PBCA fluorescence at 4 °C when no active uptake occurs, which may suggest that the particles composed of the most hydrophobic monomer associate slightly better to the cell surface. However, although we cannot exclude the possibility that increased POCA binding may partially contribute to the differential cellular responses towards the three particle variants, there was no correlation between the magnitude of POCA cell association and cellular cytotoxicity across the panel of cell lines. Although the degradation of PACA NPs is slow *in vitro* (Sulheim et al. 2016), the differential NP cytotoxicity may also be caused by release of particle-specific degradation products. Degradation of PACA particles releases cyanoacrylic acid and the corresponding alkyl alcohol, i.e. ethyl-butyl alcohol, butanol, or octanol (Vezin and Florence 1980). The differential cytotoxicity may be caused by the degree of hydrophobicity of the released alkyl alcohols. The highly hydrophobic octanol will most likely insert into the lipid bilayer and affect membrane properties to a greater extent than the hydrophilic butanol. In support of this, octanol induced calcium release and apoptosis in neural crests at *micro*molar concentrations, whereas *milli*molar concentrations of butanol were required (Garic-Stankovic et al. 2006).

NPs may not only be regarded as passive drug carriers. Emerging data indicate that various NPs' physicochemical properties and the responses induced upon interaction with biological systems could have potential in biomedicine if harnessed (Peynshaert et al. 2014). This may be extended to drug-delivery if the carrier is designed so that its biological effects are complementary with the intended drug effect. Here, we show that even minor differences in PACA NP composition leads to differential induction of cellular stress and protective pathways, and importantly, also induction of different modes of cell death. This highlights an

unexpected opportunity for fine-tuning the NP carrier effects in the direction of tailor-made precision medicine.

In conclusion, our study demonstrates that even minor differences in PACA NP composition may have significant effects on cellular responses and mode of cell death. We identified cystine availability as a key determinant of PBCA/PEBCA cytotoxicity. Importantly, PBCA particles were identified as inducers of ferroptosis, which may be exploited in drug-delivery settings. Together this demonstrates the importance of careful examination of the cellular responses to interactions between NPs and human cells for optimal exploitation of NPs in biomedicine.

Acknowledgements

We thank Tine Raabe for expert technical assistance and Ruth Schmid (SINTEF, Trondheim, Norway) for valuable discussions concerning PACA toxicity. We are grateful to Dr. Pavel Ivanov (Brigham and Women's Hospital, Boston, USA) for the HAP1 wt and eIF2α kinase knockout cell lines. The following core facilities at Oslo University Hospital are acknowledged for providing access to equipment and expertise: The Core Facility for Confocal Microscopy, the Core Facility for Flow Cytometry, and the Core Facility for Mass Spectrometry. This work was supported by The Research Council of Norway (NANO2021; project number 228200/O70, and INDNOR; project number 261093), The Norwegian Cancer Society, the University of Oslo, and the Helse Sør-Øst, Norway.

Declaration of interest statement

The authors report no conflict of interest.

References

Abdal Dayem, A., M. K. Hossain, S. B. Lee, K. Kim, S. K. Saha, G. M. Yang, H. Y. Choi, and S. G. Cho. 2017. "The Role of Reactive Oxygen Species (ROS) in the Biological Activities of Metallic Nanoparticles." *International journal of molecular sciences* 18 (1). doi:10.3390/ijms18010120

Afonyushkin, T., O. V. Oskolkova, M. Philippova, T. J. Resink, P. Erne, B. R. Binder, and V. N. Bochkov. 2010. "Oxidized phospholipids regulate expression of ATF4 and VEGF in endothelial cells via NRF2-dependent mechanism: novel point of convergence between electrophilic and unfolded protein stress pathways." *Arteriosclerosis,*

Thrombosis, and Vascular Biology 30 (5): 1007-1013. doi:10.1161/atvbaha.110.204354

Aulas, A., M. M. Fay, S. M. Lyons, C. A. Achorn, N. Kedersha, P. Anderson, and P. Ivanov. 2017. "Stress-specific differences in assembly and composition of stress granules and related foci." *Journal of Cell Science* 130 (5): 927-937. doi:10.1242/jcs.199240

Barbero, F., L. Russo, M. Vitali, J. Piella, I. Salvo, M. L. Borrajo, M. Busquets-Fite, R. Grandori, N. G. Bastus, E. Casals*, et al.* 2017. "Formation of the Protein Corona: The Interface between Nanoparticles and the Immune System." *Seminars in Immunology* 34 52-60. doi:10.1016/j.smim.2017.10.001

Bellezza, I., I. Giambanco, A. Minelli, and R. Donato. 2018. "Nrf2-Keap1 signaling in oxidative and reductive stress." *Biochimica et Biophysica Acta* 1865 (5): 721-733. doi:10.1016/j.bbamcr.2018.02.010

Cao, Y., J. Long, L. Liu, T. He, L. Jiang, C. Zhao, and Z. Li. 2017. "A review of endoplasmic reticulum (ER) stress and nanoparticle (NP) exposure." *Life Sciences* 186 33-42. doi:10.1016/j.lfs.2017.08.003

Conrad, M., J. P. Angeli, P. Vandenabeele, and B. R. Stockwell. 2016. "Regulated necrosis: disease relevance and therapeutic opportunities." *Nature Reviews: Drug Discovery* 15 (5): 348-366. doi:10.1038/nrd.2015.6

Garic-Stankovic, A., M. Hernandez, G. R. Flentke, and S. M. Smith. 2006. "Structural constraints for alcohol-stimulated Ca2+ release in neural crest, and dual agonist/antagonist properties of n-octanol." *Alcoholism, Clinical and Experimental Research* 30 (3): 552-559. doi:10.1111/j.1530-0277.2005.00061.x

Gentric, G., V. Mieulet, and F. Mechta-Grigoriou. 2017. "Heterogeneity in Cancer Metabolism: New Concepts in an Old Field." *Antioxidants and Redox Signaling* 26 (9): 462-485. doi:10.1089/ars.2016.6750

Hangauer, M. J., V. S. Viswanathan, M. J. Ryan, D. Bole, J. K. Eaton, A. Matov, J. Galeas, H. D. Dhruv, M. E. Berens, S. L. Schreiber*, et al.* 2017. "Drug-tolerant persister cancer cells are vulnerable to GPX4 inhibition." *Nature* 551 (7679): 247-250. doi:10.1038/nature24297

Hessvik, N. P., A. Overbye, A. Brech, M. L. Torgersen, I. S. Jakobsen, K. Sandvig, and A. Llorente. 2016. "PIKfyve inhibition increases exosome release and induces secretory autophagy." *Cellular and Molecular Life Sciences* 73 (24): 4717-4737. doi:10.1007/s00018-016-2309-8

Hetz, C. 2012. "The unfolded protein response: controlling cell fate decisions under ER stress and beyond." *Nature Reviews: Molecular Cell Biology* 13 (2): 89-102. doi:10.1038/nrm3270

Higashisaka, K., K. Nagano, Y. Yoshioka, and Y. Tsutsumi. 2017. "Nano-safety Research: Examining the Associations among the Biological Effects of Nanoparticles and Their Physicochemical Properties and Kinetics." *Biological and Pharmaceutical Bulletin* 40 (3): 243-248. doi:10.1248/bpb.b16-00854

Itoh, K., T. Chiba, S. Takahashi, T. Ishii, K. Igarashi, Y. Katoh, T. Oyake, N. Hayashi, K. Satoh, I. Hatayama*, et al.* 1997. "An Nrf2/small Maf heterodimer mediates the induction of phase II detoxifying enzyme genes through antioxidant response elements." *Biochemical and Biophysical Research Communications* 236 (2): 313-322. doi:10.1006/bbrc.1997.6943

Iurlaro, R., and C. Munoz-Pinedo. 2016. "Cell death induced by endoplasmic reticulum stress." *The FEBS journal* 283 (14): 2640-2652. doi:10.1111/febs.13598

Kreuter, J. 2014. "Drug delivery to the central nervous system by polymeric nanoparticles: what do we know?" *Advanced Drug Delivery Reviews* 71 2-14. doi:10.1016/j.addr.2013.08.008

Lo, M., Y. Z. Wang, and P. W. Gout. 2008. "The x(c)- cystine/glutamate antiporter: a potential target for therapy of cancer and other diseases." *Journal of Cellular Physiology* 215 (3): 593-602. doi:10.1002/jcp.21366

Lu, B., X. B. Chen, M. D. Ying, Q. J. He, J. Cao, and B. Yang. 2017. "The Role of Ferroptosis in Cancer Development and Treatment Response." *Frontiers in Pharmacology* 8 992. doi:10.3389/fphar.2017.00992

Lu, L., A. P. Han, and J. J. Chen. 2001. "Translation initiation control by heme-regulated eukaryotic initiation factor 2alpha kinase in erythroid cells under cytoplasmic stresses." *Molecular and Cellular Biology* 21 (23): 7971-7980. doi:10.1128/mcb.21.23.7971-7980.2001

Miyamoto, N., H. Izumi, R. Miyamoto, H. Bin, H. Kondo, A. Tawara, Y. Sasaguri, and K. Kohno. 2011. "Transcriptional regulation of activating transcription factor 4 under oxidative stress in retinal pigment epithelial ARPE-19/HPV-16 cells." *Investigative Ophthalmology and Visual Science* 52 (3): 1226-1234. doi:10.1167/iovs.10-5775

Morata-Tarifa, C., G. Jimenez, M. A. Garcia, J. M. Entrena, C. Grinan-Lison, M. Aguilera, M. Picon-Ruiz, and J. A. Marchal. 2016. "Low adherent cancer cell subpopulations are enriched in tumorigenic and metastatic epithelial-to-mesenchymal transition-induced cancer stem-like cells." *Scientific Reports* 6 18772. doi:10.1038/srep18772

Morch, Y., R. Hansen, S. Berg, A. K. Aslund, W. R. Glomm, S. Eggen, R. Schmid, H. Johnsen, S. Kubowicz, S. Snipstad*, et al.* 2015. "Nanoparticle-stabilized microbubbles for multimodal imaging and drug delivery." *Contrast media & molecular imaging* 10 (5): 356-366. doi:10.1002/cmmi.1639

Mouritsen, O. G. 2011. "Lipids, curvature, and nano-medicine." *European Journal of Lipid Science and Technology* 113 (10): 1174-1187. doi:10.1002/ejlt.201100050

Narang, V. S., G. M. Pauletti, P. W. Gout, D. J. Buckley, and A. R. Buckley. 2007. "Sulfasalazine-induced reduction of glutathione levels in breast cancer cells: enhancement of growth-inhibitory activity of Doxorubicin." *Chemotherapy* 53 (3): 210-217. doi:10.1159/000100812

Nel, A. E., L. Madler, D. Velegol, T. Xia, E. M. Hoek, P. Somasundaran, F. Klaessig, V. Castranova, and M. Thompson. 2009. "Understanding biophysicochemical interactions at the nano-bio interface." *Nature Materials* 8 (7): 543-557. doi:10.1038/nmat2442

Pakos-Zebrucka, K., I. Koryga, K. Mnich, M. Ljujic, A. Samali, and A. M. Gorman. 2016. "The integrated stress response." *EMBO reports* 17 (10): 1374-1395. doi:10.15252/embr.201642195

Peynshaert, K., B. B. Manshian, F. Joris, K. Braeckmans, S. C. De Smedt, J. Demeester, and S. J. Soenen. 2014. "Exploiting intrinsic nanoparticle toxicity: the pros and cons of nanoparticle-induced autophagy in biomedical research." *Chemical Reviews* 114 (15): 7581-7609. doi:10.1021/cr400372p

Sarhan, M., A. von Massenhausen, C. Hugo, R. Oberbauer, and A. Linkermann. 2018. "Immunological consequences of kidney cell death." *Cell Death & Disease* 9 (2): 114. doi:10.1038/s41419-017-0057-9

Sato, M., R. Kusumi, S. Hamashima, S. Kobayashi, S. Sasaki, Y. Komiyama, T. Izumikawa, M. Conrad, S. Bannai, and H. Sato. 2018. "The ferroptosis inducer erastin irreversibly inhibits system xc- and synergizes with cisplatin to increase cisplatin's cytotoxicity in cancer cells." *Scientific Reports* 8 (1): 968. doi:10.1038/s41598-018-19213-4

Senft, A. P., T. P. Dalton, and H. G. Shertzer. 2000. "Determining glutathione and glutathione disulfide using the fluorescence probe o-phthalaldehyde." *Analytical Biochemistry* 280 (1): 80-86. doi:10.1006/abio.2000.4498

Sidrauski, C., D. Acosta-Alvear, A. Khoutorsky, P. Vedantham, B. R. Hearn, H. Li, K. Gamache, C. M. Gallagher, K. K. Ang, C. Wilson*, et al.* 2013. "Pharmacological brake-release of mRNA translation enhances cognitive memory." *Elife* 2 e00498. doi:10.7554/eLife.00498

Sies, H., C. Berndt, and D. P. Jones. 2017. "Oxidative Stress." *Annual Review of Biochemistry* 86 715-748. doi:10.1146/annurev-biochem-061516-045037

Simon, J., T. Wolf, K. Klein, K. Landfester, V. Mailander, and F. R. Wurm. 2018. "Hydrophilicity regulates the stealth properties of polyphosphoester-coated nanocarriers." *Angewandte Chemie. International Ed. In English*. doi:10.1002/anie.201800272

Snipstad, S., S. Berg, Y. Morch, A. Bjorkoy, E. Sulheim, R. Hansen, I. Grimstad, A. van Wamel, A. F. Maaland, S. H. Torp*, et al.* 2017. "Ultrasound Improves the Delivery and Therapeutic Effect of Nanoparticle-Stabilized Microbubbles in Breast Cancer Xenografts." *Ultrasound in Medicine and Biology* 43 (11): 2651-2669. doi:10.1016/j.ultrasmedbio.2017.06.029

Starheim, K. K., T. Holien, K. Misund, I. Johansson, K. A. Baranowska, A. M. Sponaas, H. Hella, G. Buene, A. Waage, A. Sundan*, et al.* 2016. "Intracellular glutathione determines bortezomib cytotoxicity in multiple myeloma cells." *Blood cancer journal* 6 (7): e446. doi:10.1038/bcj.2016.56

Stockwell, B. R., J. P. Friedmann Angeli, H. Bayir, A. I. Bush, M. Conrad, S. J. Dixon, S. Fulda, S. Gascon, S. K. Hatzios, V. E. Kagan*, et al.* 2017. "Ferroptosis: A Regulated Cell Death Nexus Linking Metabolism, Redox Biology, and Disease." *Cell* 171 (2): 273-285. doi:10.1016/j.cell.2017.09.021

Sukhanova, A., S. Bozrova, P. Sokolov, M. Berestovoy, A. Karaulov, and I. Nabiev. 2018. "Dependence of Nanoparticle Toxicity on Their Physical and Chemical Properties." *Nanoscale research letters* 13 (1): 44. doi:10.1186/s11671-018-2457-x

Sulheim, E., H. Baghirov, E. von Haartman, A. Boe, A. K. Aslund, Y. Morch, and L. Davies Cde. 2016. "Cellular uptake and intracellular degradation of poly(alkyl cyanoacrylate) nanoparticles." *Journal of nanobiotechnology* 14 1. doi:10.1186/s12951-015-0156-7

Sulheim, E., T. G. Iversen, V. To Nakstad, G. Klinkenberg, H. Sletta, R. Schmid, A. R. Hatletveit, A. M. Wagbo, A. Sundan, T. Skotland*, et al.* 2017. "Cytotoxicity of Poly(Alkyl Cyanoacrylate) Nanoparticles." *International journal of molecular sciences* 18 (11). doi:10.3390/ijms18112454

Thastrup, O., P. J. Cullen, B. K. Drobak, M. R. Hanley, and A. P. Dawson. 1990. "Thapsigargin, a tumor promoter, discharges intracellular Ca2+ stores by specific inhibition of the endoplasmic reticulum Ca2(+)-ATPase." *Proceedings of the National Academy of Sciences of the United States of America* 87 (7): 2466-2470.

Timmerman, L. A., T. Holton, M. Yuneva, R. J. Louie, M. Padro, A. Daemen, M. Hu, D. A. Chan, S. P. Ethier, L. J. van 't Veer*, et al.* 2013. "Glutamine sensitivity analysis identifies the xCT antiporter as a common triple-negative breast tumor therapeutic target." *Cancer Cell* 24 (4): 450-465. doi:10.1016/j.ccr.2013.08.020

van Zandwijk, N. 1995. "N-acetylcysteine (NAC) and glutathione (GSH): antioxidant and chemopreventive properties, with special reference to lung cancer." *Journal of Cellular Biochemistry. Supplement* 22 24-32.

Vauthier, C., C. Dubernet, E. Fattal, H. Pinto-Alphandary, and P. Couvreur. 2003. "Poly(alkylcyanoacrylates) as biodegradable materials for biomedical applications." *Advanced Drug Delivery Reviews* 55 (4): 519-548. doi:10.1016/S0169-409X(03)00041-3

Vezin, W. R., and A. T. Florence. 1980. "In vitro heterogeneous degradation of poly(n-alkyl alpha-cyanoacrylates)." *Journal of Biomedical Materials Research* 14 (2): 93-106. doi:10.1002/jbm.820140202

Viswanathan, V. S., M. J. Ryan, H. D. Dhruv, S. Gill, O. M. Eichhoff, B. Seashore-Ludlow, S. D. Kaffenberger, J. K. Eaton, K. Shimada, A. J. Aguirre*, et al.* 2017. "Dependency of a therapy-resistant state of cancer cells on a lipid peroxidase pathway." *Nature* 547 (7664): 453-457. doi:10.1038/nature23007

White, M. C., R. D. Schroeder, K. Zhu, K. Xiong, and D. J. McConkey. 2018. "HRI-mediated translational repression reduces proteotoxicity and sensitivity to bortezomib in human pancreatic cancer cells." *Oncogene*. doi:10.1038/s41388-018-0227-y

Yu, H., P. Guo, X. Xie, Y. Wang, and G. Chen. 2017. "Ferroptosis, a new form of cell death, and its relationships with tumourous diseases." *Journal of Cellular and Molecular Medicine* 21 (4): 648-657. doi:10.1111/jcmm.13008

Yu, X., and Y. C. Long. 2016. "Crosstalk between cystine and glutathione is critical for the regulation of amino acid signaling pathways and ferroptosis." *Scientific Reports* 6 30033. doi:10.1038/srep30033

Zilka, O., R. Shah, B. Li, J. P. Friedmann Angeli, M. Griesser, M. Conrad, and D. A. Pratt. 2017. "On the Mechanism of Cytoprotection by Ferrostatin-1 and Liproxstatin-1 and the Role of Lipid Peroxidation in Ferroptotic Cell Death." *ACS central science* 3 (3): 232-243. doi:10.1021/acscentsci.7b00028

Figure legends

Figure 1. Highly similar PACA particles induce differential cytotoxicity and heat shock response. A. Schematic overview of the major NP-induced cellular stress responses that contribute to the final outcome of NP-cell interactions. **B.** Molecular structure of the highly similar alkylcyanoacrylate monomers used in this study, and physicochemical characteristics of the resulting NPs. **C.** Cell viability after 24 hours of treatment with PEBCA, PBCA or POCA particles was assessed by determining the cellular ATP levels. All values were normalized to that of untreated control cells. **D.** The indicated cell lines were treated with PEBCA, PBCA or POCA particles (25 μg ml^{-1}) for the indicated times and cell lysates were prepared for immunoblotting. The blots were probed with the indicated antibodies. **E.** Relative expression of selected heat shock proteins after treatment of HCT116 cells with PEBCA, PBCA or POCA particles (25 μg ml^{-1}, 4 hours). The graphs show mean values ± SEM quantified from at least three independent experiments, except the MS data that originate from triplicate samples from one experiment. The asterisks denote the statistical significances compared to untreated control. *, $p < 0.05$; **, $p < 0.01$; ***, $p < 0.001$.

Figure 2. The PACA particles differentially activate ER stress and the integrated stress response. A. Schematic overview of the IRE1 ER stress pathway and the common pathway downstream of the four eIF2α kinases PERK, GCN2, HRI and PKR that sense cellular stress such as ER stress, starvation, oxidative stress, unfolded/misfolded proteins, or viral RNA. The downstream effects of phospho-eIF2α are inhibited by ISRIB. **B.** The indicated cell lines were treated with PEBCA, PBCA, or POCA particles (25 μg ml^{-1}) for the indicated times and cell lysates were prepared for immunoblotting. The blots were probed with the indicated antibodies, and representative blots are shown. The asterisks indicate an unspecific band. **C**. MDA-MB-231 cells were treated with PBCA particles (25 μg ml^{-1}) in the absence or presence of ISRIB (100 nM) and cell lysates were prepared for immunoblotting. Thapsigargin (TG, 100 nM, 4 hours) was used as a positive control. The levels of phospho-eIF2α and ATF4 were normalized to total eIF2α and presented as percent of Ctrl (**D**). **E**. Relative protein synthesis in MDA-MB-231 cells measured by incorporation of [^{3}H]leucine for 20 minutes after treatment with PBCA particles (25 μg ml^{-1}) for the indicated times in the absence or presence of ISRIB (100 nM). **F**. MDA-MB-231 cells were transfected with either non-targeting control siRNA

(siCtrl) or two independent siRNAs targeting HRI, PERK, GCN2, or PKR. After 48 hours the cells were treated with PBCA particles (25 μg ml^{-1}) for the indicated times and cell lysates were prepared for immunoblotting. The blots were probed with the indicated antibodies. **G**. HAP1 WT, ΔHRI, ΔPERK, ΔGCN2, or ΔPKR cells were treated with PBCA (25 μg ml^{-1}) for the indicated times and cell lysates were prepared for immunoblotting. **H**. Quantification of data from the 1 hour time point. The ratio of p-eIF2α to total eIF2α was normalized to the maximum value within each experiment. All bars show mean values ± SEM quantified from at least three independent experiments. *, $p < 0.05$; **, $p < 0.01$.

Figure 3. POCA particles selectively induce apoptotic cell death. A. The panel of cell lines was treated with the indicated concentrations of PEBCA, PBCA, or POCA particles for 24 hours and cell lysates were prepared for immunoblotting. Detached cells were collected and included in the lysates, and equal volumes of non-normalized lysates were loaded on the gel to visualize an eventual loss of material due to cell death. The blots were probed with the indicated antibodies, and apoptosis is indicated by cleaved PARP (cl. PARP) and cleaved caspase-3 (cl. caspase-3). **B**. Apoptotic and necrotic cell death was assessed in Huh7 and MDA-MB-231 cells treated with the indicated concentrations of PEBCA, PBCA or POCA particles for up to 18 hours by employing the fluorogenic substrate CellEvent™ Caspase 3/7 and the cell-impermeable dye propidium iodide. The indicated time points (hours) are shown. For full movies, see Supplementary Movies 1-6. Scale bar 10 μm. **C.** Cell viability of MDA-MB-231 cells after 24 hours of treatment with POCA or PBCA particles in the absence or presence of z-VAD (20 μM) was assessed by determining the cellular ATP levels. The graphs show mean values ± SEM quantified from at least three independent experiments *, $p < 0.05$; **, $p < 0.01$.

Figure 4. PBCA particles induce ferroptosis, GSH depletion and lipid peroxidation in MDA-MB-231 cells. A. Schematic overview of inducers and inhibitors of ferroptotic cell death. **B-C**. Cytotoxicity assessed by CellTox Green staining of MDA-MB-231 cells treated with PBCA particles (50 μg ml^{-1}, 24 hours) in the presence or absence of liproxstatin (Liprox, 1 μM), ferrostatin (Fer, 2 μM), deferiprone (DFP, 100 μM), or z-VAD (20 μM). **D**. The cellular ROS level was assessed by CM-H_2DCFDA fluorescence after treatment of MDA-MB-231 cells with PEBCA, PBCA or POCA particles (25 μg ml^{-1}) for 30 minutes in the

absence or presence of N-acetyl cysteine (NAC, 5 mM). H_2O_2 (100 μM) was used as positive control. **E.** The intracellular concentration of reduced glutathione (GSH) was determined with o-phthalaldehyde in cells treated with PBCA particles (25 μg ml^{-1}) for the indicated times. Inhibition of glutathione synthesis by buthionine sulfoximine (BSO, 100 μM) for 18 hours was used as a positive control for GSH depletion. **F.** MDA-MB-231 cells were treated with PBCA (25 μg ml^{-1}) in the absence or presence of reduced glutathione (GSH, 10 mM) for the indicated times and lysates were prepared for immunoblotting. The blots were probed with the indicated antibodies, and representative blots are shown. **G.** Cell viability assessed by ATP levels of MDA-MB-231 cells treated with PBCA or POCA particles for 24 hours in the absence or presence of either GSH (10 mM) or NAC (5 mM). **H**. Flow cytometric determination of BODIPY-C11 staining of MDA-MB-231 cells after 4 hours treatment with the indicated concentrations (μg ml^{-1}) of PBCA in the absence or presence of liproxstatin (1 μM). All graphs show mean values ± SEM quantified from at least three independent experiments. The asterisks denote the statistical significances compared to untreated control, unless otherwise indicated. *, $p < 0.05$; **, $p < 0.01$; ***, $p < 0.001$.

Figure 5. Both PEBCA and PBCA particles promote ferroptosis under cystine-starvation conditions. A. Schematic overview of the relationship between cystine import through the cystine transporter SLC7A11 and the transcription factors ATF4 and Nrf2 in ferroptosis. **B-C.** Cytotoxicity assessed by CellTox Green staining of MDA-MB-231 cells treated with PBCA or PEBCA particles (12.5 μg ml^{-1}, 24 hours) in full medium or in cystine-free medium in the presence or absence of liproxstatin (Liprox, 1 μM), ferrostatin (Fer, 2 μM), deferiprone (DFP, 100 μM), z-VAD (20 μM), or cystine (200 μM). **D**. Cellular glutathione levels were determined in cells treated with PEBCA or PBCA particles (12.5 μg ml^{-1}, 4 h) in cystine-free medium. **E**. Flow cytometric determination of BODIPY-C11 staining of MDA-MB-231 cells after 4 hours treatment with the indicated concentrations (μg ml^{-1}) of PEBCA or PBCA in cystine-free medium in the absence or presence of liproxstatin (1 μM). **F**. Cell viability assessed as ATP levels of MDA-MB-231 cells depleted for ATF4 for 48 hours and then treated with PBCA particles for 24 hours. The data were normalized to the respective non-particle-treated control for each siRNA. Depletion of ATF4 by itself did not alter the viability of untreated control cells. **G**. Transcription of *ATF4* mRNA in cells treated with the indicated concentrations of PEBCA or PBCA particles for 4 hours. **H-I**. Cells were treated with PEBCA or PBCA particles (12.5 μg ml^{-1}) for 4 hours in full- or cystine-free

medium and cell lysates were prepared for immunoblotting. The relative level of ATF4 was normalized to eIF2α. **J**. Transcription of *SLC7A11* mRNA in cells transfected with a non-targeting control siRNA (siCtrl) or by two independent siRNAs targeting ATF4. 48 hours later the cells were treated with PEBCA (50 μg ml^{-1}) or PBCA (12.5 μg ml^{-1}) for 4 hours. All graphs show mean values ± SEM quantified from at least three independent experiments. The asterisks denote the statistical significances compared to untreated control, unless otherwise indicated. *, $p < 0.05$; **, $p < 0.01$; ***, $p < 0.001$.

Figure 6. PEBCA- and PBCA-induced accumulation of ATF4 and Nrf2 counteracts ferroptosis in MDA-MB-231 cells. A. MDA-MB-231 cells were treated with the indicated concentrations of PEBCA, PBCA or POCA for 4, 8 or 16 hours and cell lysates were prepared for immunoblotting. The relative levels of Nrf2 at 4 and 8 hours were normalized to eIF2α (lower panels). **B**. MDA-MB-231 cells were transfected with a non-targeting siRNA (siCtrl) or two independent siRNAs targeting Nrf2. 48 hours later the cells were stimulated with PEBCA particles (50 μg ml^{-1}) for 6 hours to demonstrate efficient knockdown of Nrf2. **C**. Cell viability assessed as ATP levels of MDA-MB-231 cells transfected with a non-targeting control siRNA or by two independent siRNAs targeting Nrf2 and 48 hours later treated with PEBCA or PBCA particles for 24 hours. The data were normalized to the respective non-particle-treated control for each siRNA. Depletion of Nrf2 by itself only reduced the viability of untreated control cells by ~20%. The curves were extended to 100% viability to simplify comparison between siCtrl and siNrf2. The asterisks denote the statistical significance between siCtrl and each siNrf2 oligo at the respective PACA concentrations. **D-E**. Cytotoxicity assessed by CellTox Green staining of MDA-MB-231 cells depleted for Nrf2 and subsequently treated with PBCA or PEBCA particles (12.5 μg ml^{-1}, 24 hours) in the presence or absence of liproxstatin (Liprox, 1 μM), ferrostatin (Fer, 2 μM), deferiprone (DFP, 100 μM), or z-VAD (20 μM). **F**. Transcription of *SLC7A11* in cells transfected with a non-targeting control siRNA (siCtrl) or by two independent siRNAs targeting Nrf2 and 48 hours later treated with PEBCA (50 μg ml^{-1}) or PBCA (12.5 μg ml^{-1}) for 4 hours. **G**. MDA-MB-231 cells were transfected with a non-targeting siRNA or two independent siRNAs targeting SLC7A11. Lysates were prepared for immunoblotting 48 hours later. **H**. Cell viability assessed as ATP levels of MDA-MB-231 cells transfected with a non-targeting control siRNA (siCtrl) or by two independent siRNAs targeting SLC7A11 and 48 hours later treated with PEBCA or PBCA particles for 24 hours. The data were normalized to the respective non-

particle-treated control for each siRNA. Depletion of SLC7A11 by itself only reduced the viability of untreated control cells by ~15%. The curves were extended to 100% viability to simplify comparison between siCtrl and siSLC7A11. The asterisks denote the statistical significance between siCtrl and each siSLC7A11 oligo at the respective PBCA concentrations. **I-J**. Cytotoxicity assessed by CellTox Green staining of MDA-MB-231 cells depleted for SLC7A11 and 48 hours later treated with PBCA or PEBCA particles (12.5 μg ml^{-1}, 24 hours) in the presence or absence of liproxstatin (Liprox, 1 μM), ferrostatin (Fer, 2 μM), deferiprone (DFP, 100 μM), z-VAD (20 μM), or β-mercaptoethanol (β-ME, 50 μM). **K**. Schematic overview of cellular import of the dimer cystine and the monomer cysteine. All graphs show mean values ± SEM quantified from at least three independent experiments, except Fig. 6H PEBCA (n=2). The asterisks denote the statistical significances compared to untreated control, unless otherwise indicated. *, $p < 0.05$; **, $p < 0.01$; ***, $p < 0.001$.

Figure 1.

A

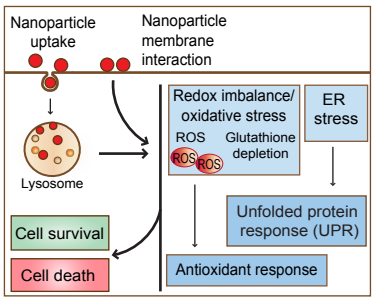

B

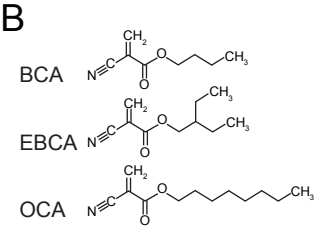

Monomer	NP size	PDI	ζ-potential
BCA	133 ± 16	0.13 ± 0.03	-3.4 ± 0.5
EBCA	150 ± 14	0.15 ± 0.04	-2.4 ± 0.5
OCA	153 ± 25	0.16 ± 0.05	-3.3 ± 2.1

C

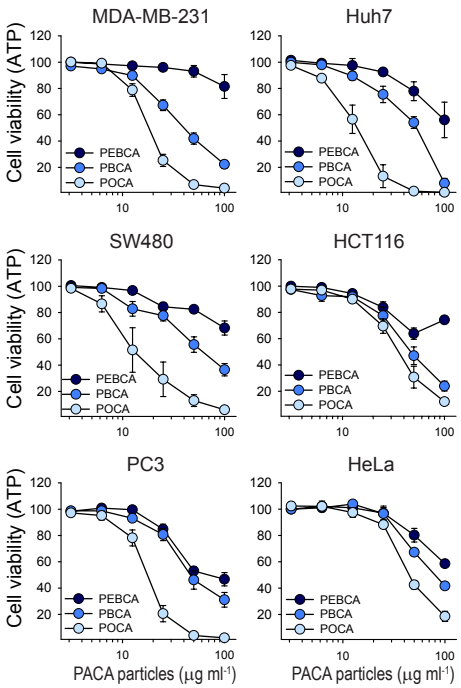

D

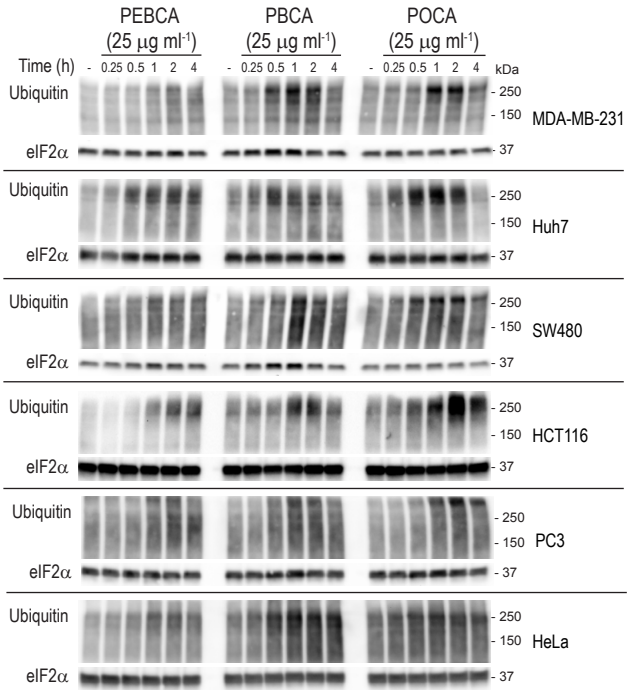

E

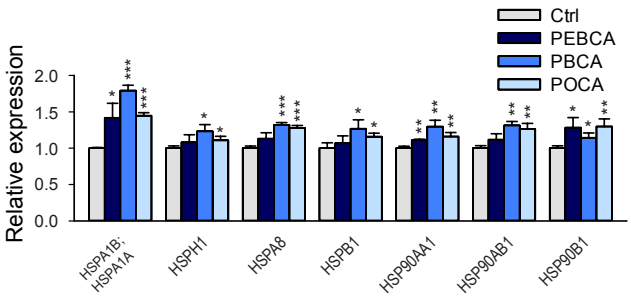

Figure 2.

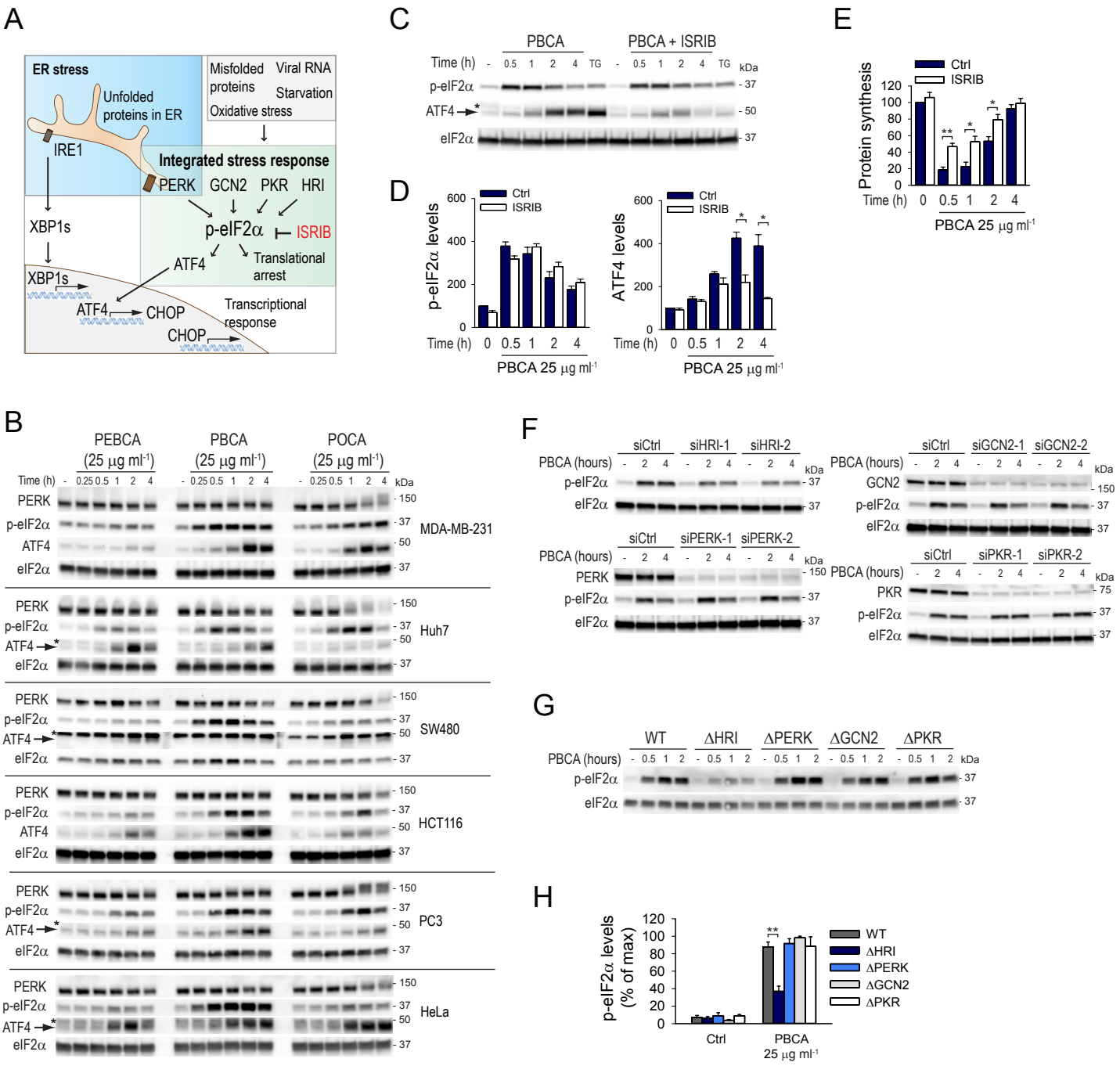
A
ER stress
Unfolded proteins in ER
IRE1
XBP1s
XBP1s
ATF4
CHOP
CHOP
Misfolded proteins
Viral RNA
Starvation
Oxidative stress
Integrated stress response
PERK
GCN2
PKR
HRI
p-eIF2α
ISRIB
ATF4
Translational arrest
Transcriptional response
C
PBCA
PBCA + ISRIB
Time (h)
p-eIF2α
ATF4
eIF2α
kDa
D
Ctrl
ISRIB
p-eIF2α levels
ATF4 levels
Time (h)
PBCA 25 μg ml-1
E
Protein synthesis
Ctrl
ISRIB
Time (h)
PBCA 25 μg ml-1
B
PEBCA (25 μg ml-1)
PBCA (25 μg ml-1)
POCA (25 μg ml-1)
Time (h)
PERK
p-eIF2α
ATF4
eIF2α
MDA-MB-231
Huh7
SW480
HCT116
PC3
HeLa
F
siCtrl
siHRI-1
siHRI-2
siPERK-1
siPERK-2
siGCN2-1
siGCN2-2
siPKR-1
siPKR-2
PBCA (hours)
GCN2
PKR
G
WT
ΔHRI
ΔPERK
ΔGCN2
ΔPKR
H
p-eIF2α levels (% of max)
Ctrl
PBCA 25 μg ml-1

Figure 3.

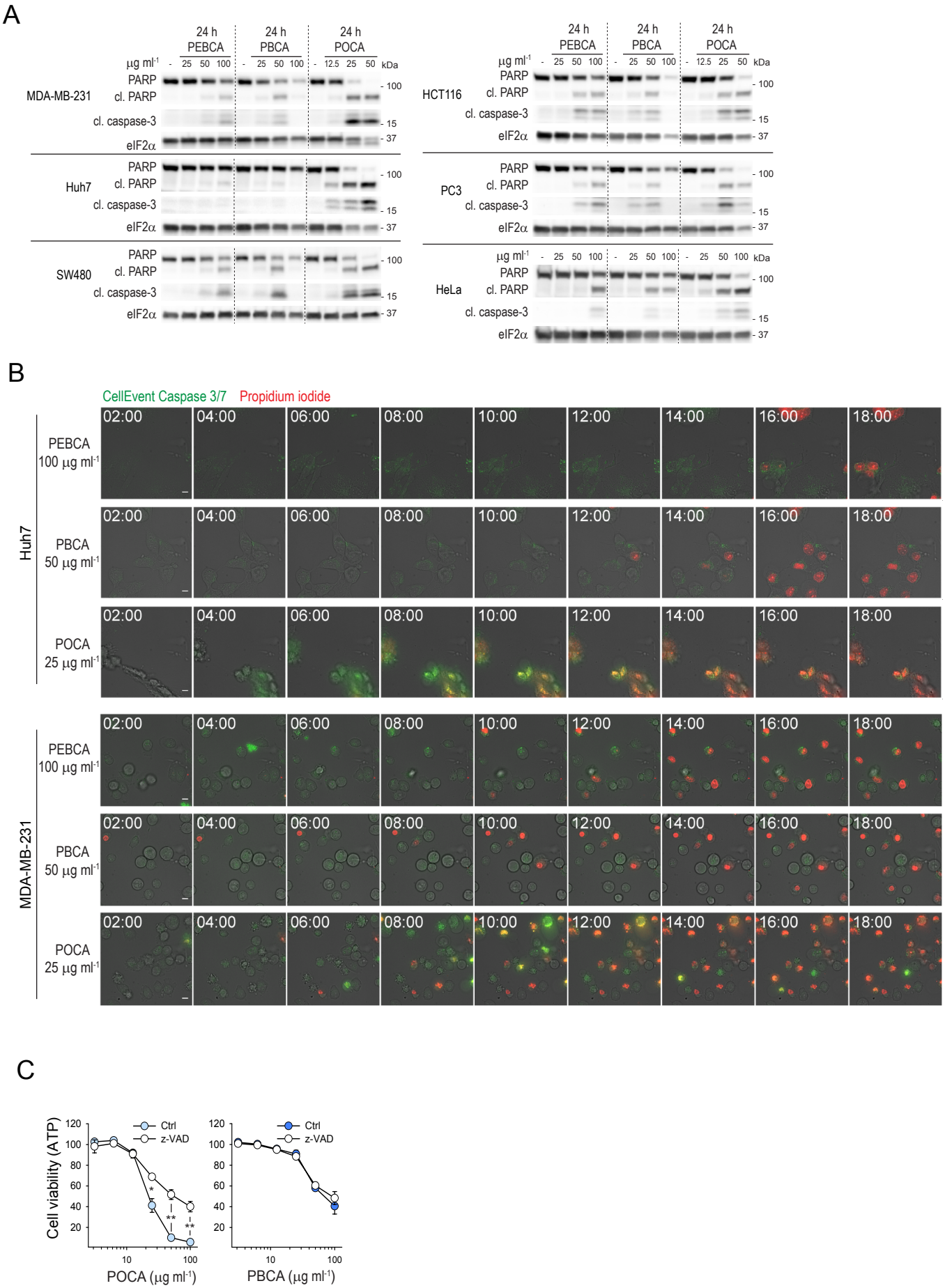
A
24 h PEBCA
24 h PBCA
24 h POCA
μg ml-1
kDa
MDA-MB-231
HCT116
Huh7
PC3
SW480
HeLa
PARP
cl. PARP
cl. caspase-3
eIF2α
B
CellEvent Caspase 3/7
Propidium iodide
Huh7
MDA-MB-231
PEBCA 100 μg ml-1
PBCA 50 μg ml-1
POCA 25 μg ml-1
C
Cell viability (ATP)
Ctrl
z-VAD
POCA (μg ml-1)
PBCA (μg ml-1)

Figure 4.

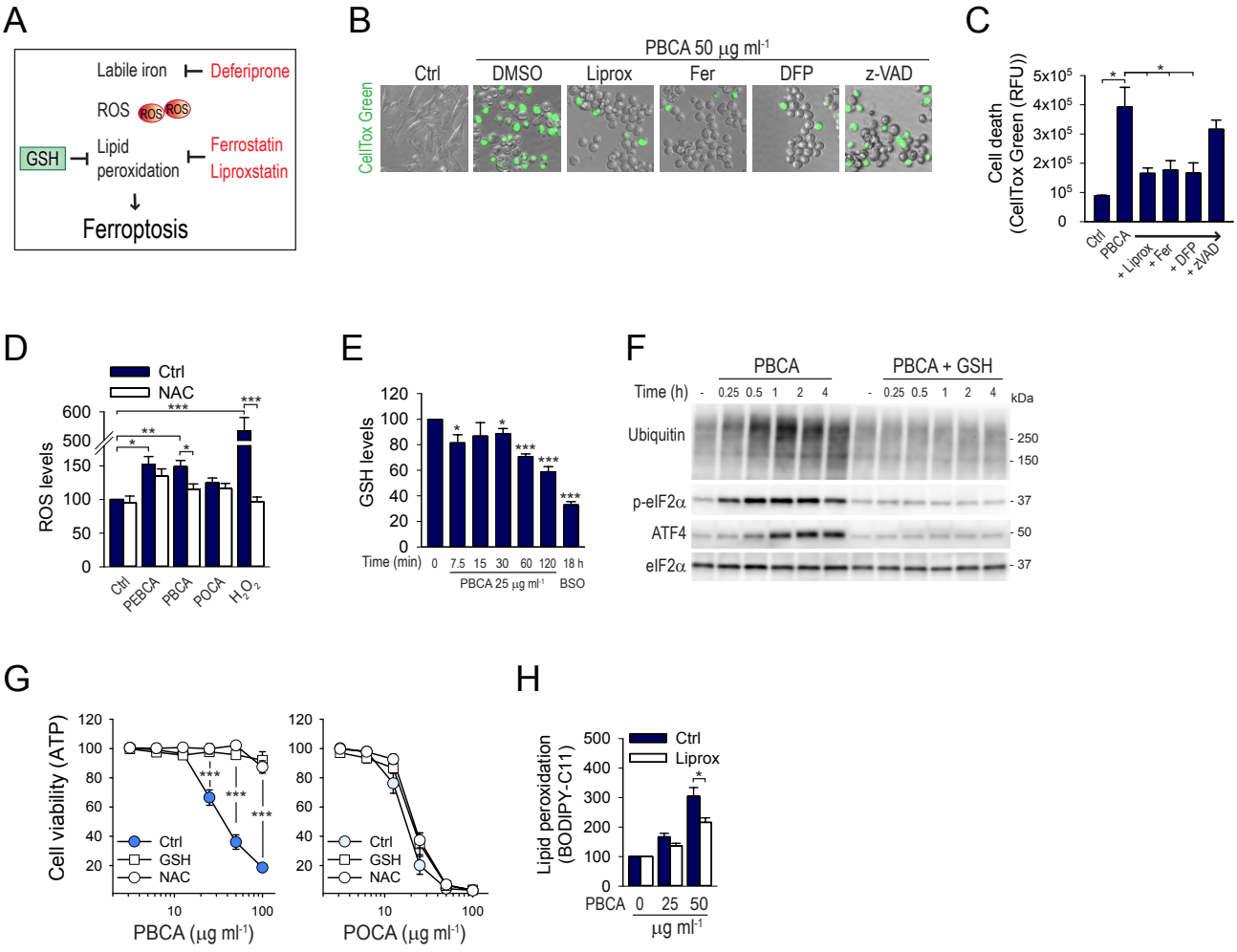
A
Labile iron
Deferiprone
ROS
GSH
Lipid peroxidation
Ferrostatin
Liproxstatin
Ferroptosis
B
PBCA 50 μg ml-1
Ctrl
DMSO
Liprox
Fer
DFP
z-VAD
CellTox Green
C
Cell death (CellTox Green (RFU))
Ctrl
PBCA
+ Liprox
+ Fer
+ DFP
+ zVAD
D
Ctrl
NAC
ROS levels
Ctrl
PEBCA
PBCA
POCA
H2O2
E
GSH levels
Time (min)
PBCA 25 μg ml-1
BSO
F
PBCA
PBCA + GSH
Time (h)
kDa
Ubiquitin
p-eIF2α
ATF4
eIF2α
G
Cell viability (ATP)
Ctrl
GSH
NAC
PBCA (μg ml-1)
POCA (μg ml-1)
H
Lipid peroxidation (BODIPY-C11)
Ctrl
Liprox
PBCA
μg ml-1

Figure 5.

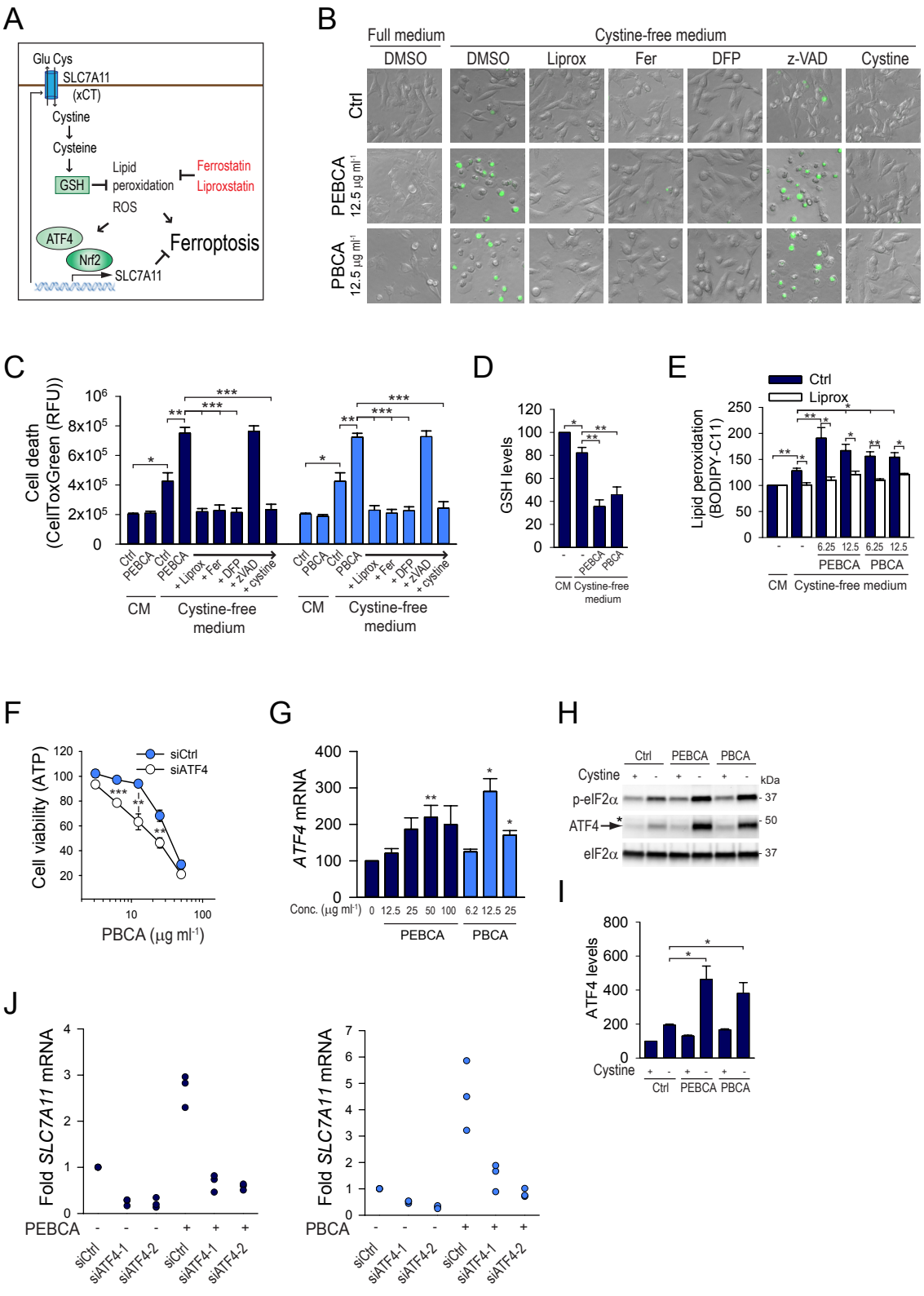
A
Glu Cys
SLC7A11
(xCT)
Cystine
Cysteine
GSH
Lipid peroxidation
ROS
Ferrostatin
Liproxstatin
ATF4
Nrf2
SLC7A11
Ferroptosis
B
Full medium
Cystine-free medium
DMSO
DMSO
Liprox
Fer
DFP
z-VAD
Cystine
Ctrl
PEBCA 12.5 μg ml-1
PBCA 12.5 μg ml-1
C
Cell death (CellToxGreen (RFU))
Ctrl
PEBCA
PBCA
+ Liprox
+ Fer
+ DFP
+ z-VAD
+ cystine
CM
Cystine-free medium
D
GSH levels
CM
Cystine-free medium
E
Ctrl
Liprox
Lipid peroxidation (BODIPY-C11)
6.25
12.5
PEBCA
PBCA
CM
Cystine-free medium
F
siCtrl
siATF4
Cell viability (ATP)
PBCA (μg ml-1)
G
ATF4 mRNA
Conc. (μg ml-1)
PEBCA
PBCA
H
Ctrl
PEBCA
PBCA
Cystine
p-eIF2α
ATF4
eIF2α
kDa
I
ATF4 levels
Cystine
Ctrl
PEBCA
PBCA
J
Fold SLC7A11 mRNA
PEBCA
PBCA
siCtrl
siATF4-1
siATF4-2

Figure 6.

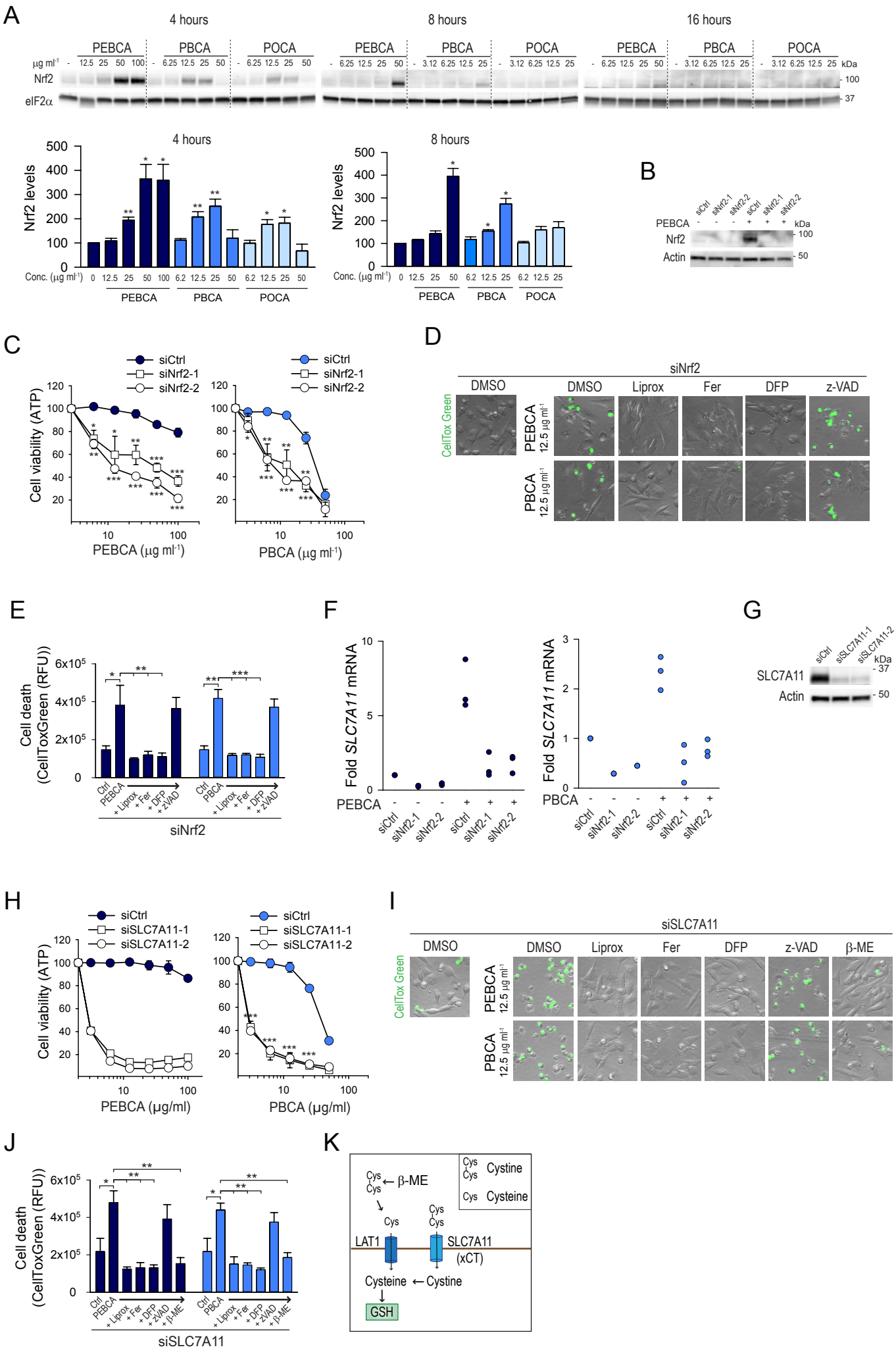
A
4 hours
8 hours
16 hours
PEBCA
PBCA
POCA
Nrf2
eIF2α
kDa
100
37
Nrf2 levels
Conc. (μg ml-1)
B
siCtrl
siNrf2-1
siNrf2-2
Actin
50
C
Cell viability (ATP)
PEBCA (μg ml-1)
PBCA (μg ml-1)
D
siNrf2
DMSO
Liprox
Fer
DFP
z-VAD
CellTox Green
E
Cell death (CellToxGreen (RFU))
siNrf2
F
Fold SLC7A11 mRNA
G
SLC7A11
H
PEBCA (μg/ml)
PBCA (μg/ml)
I
siSLC7A11
β-ME
J
siSLC7A11
K
Cystine
Cysteine
LAT1
SLC7A11
(xCT)
GSH

Supplementary Figure 1.

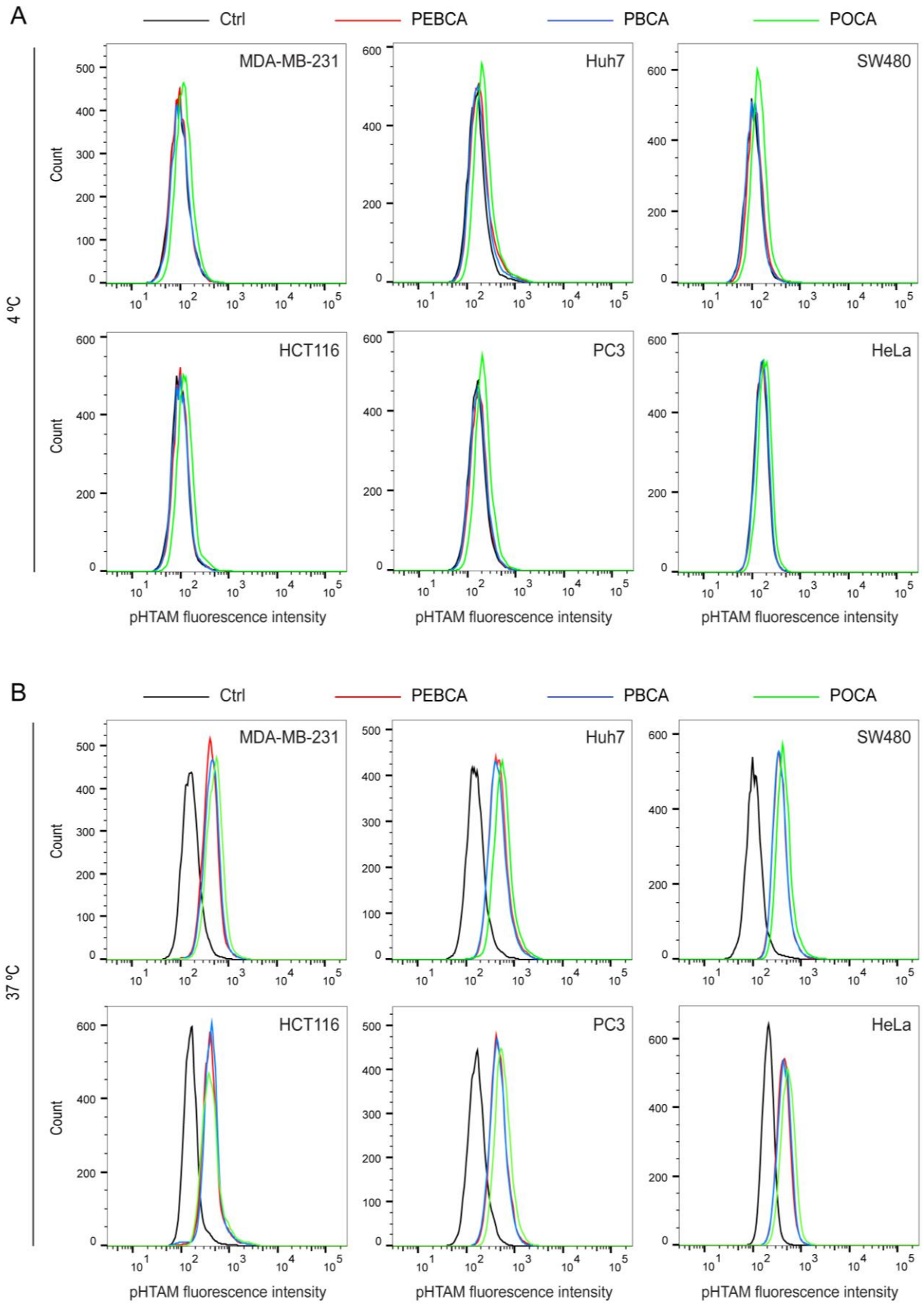

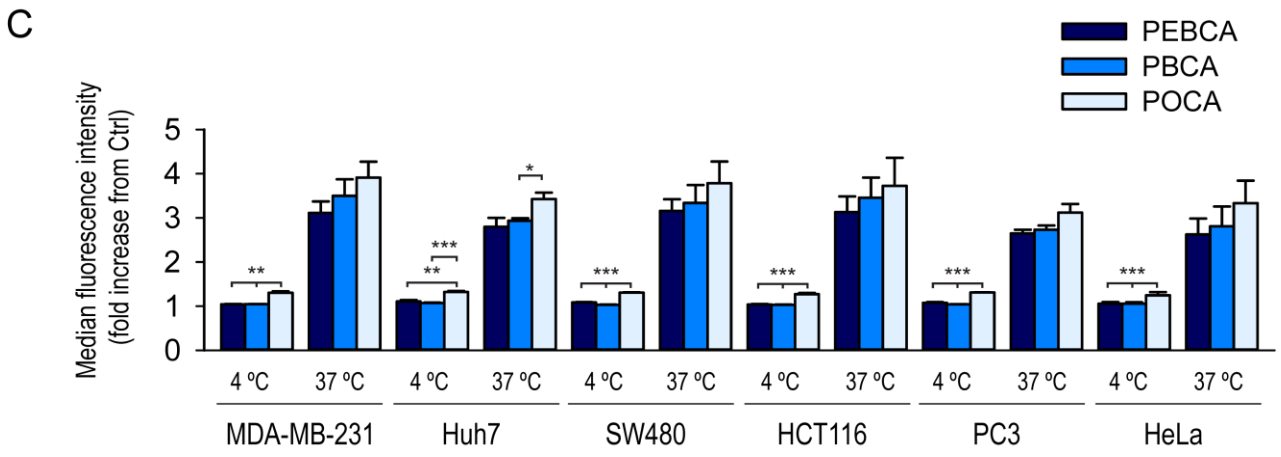

Supplementary Figure 1. Cellular association of PEBCA, PBCA and POCA particles. The panel of cell lines was treated with 25 μg ml^{-1} of PEBCA, PBCA and POCA particles for 2 hours at either 4 °C (**A**) or at 37 °C (**B**). The cells were washed three times in PBS, detached by Accutase™ and washed again before the PACA particle fluorescence was detected by flow cytometry. At least 10,000 viable cells were counted for each condition. Representative histograms are shown. **C**. The median fluorescence intensity from at least 10,000 viable cells was determined for each condition and the fold increase compared to untreated control cells was calculated. The data are presented as mean values ± SEM from three independent experiments.

Supplementary Figure 2.

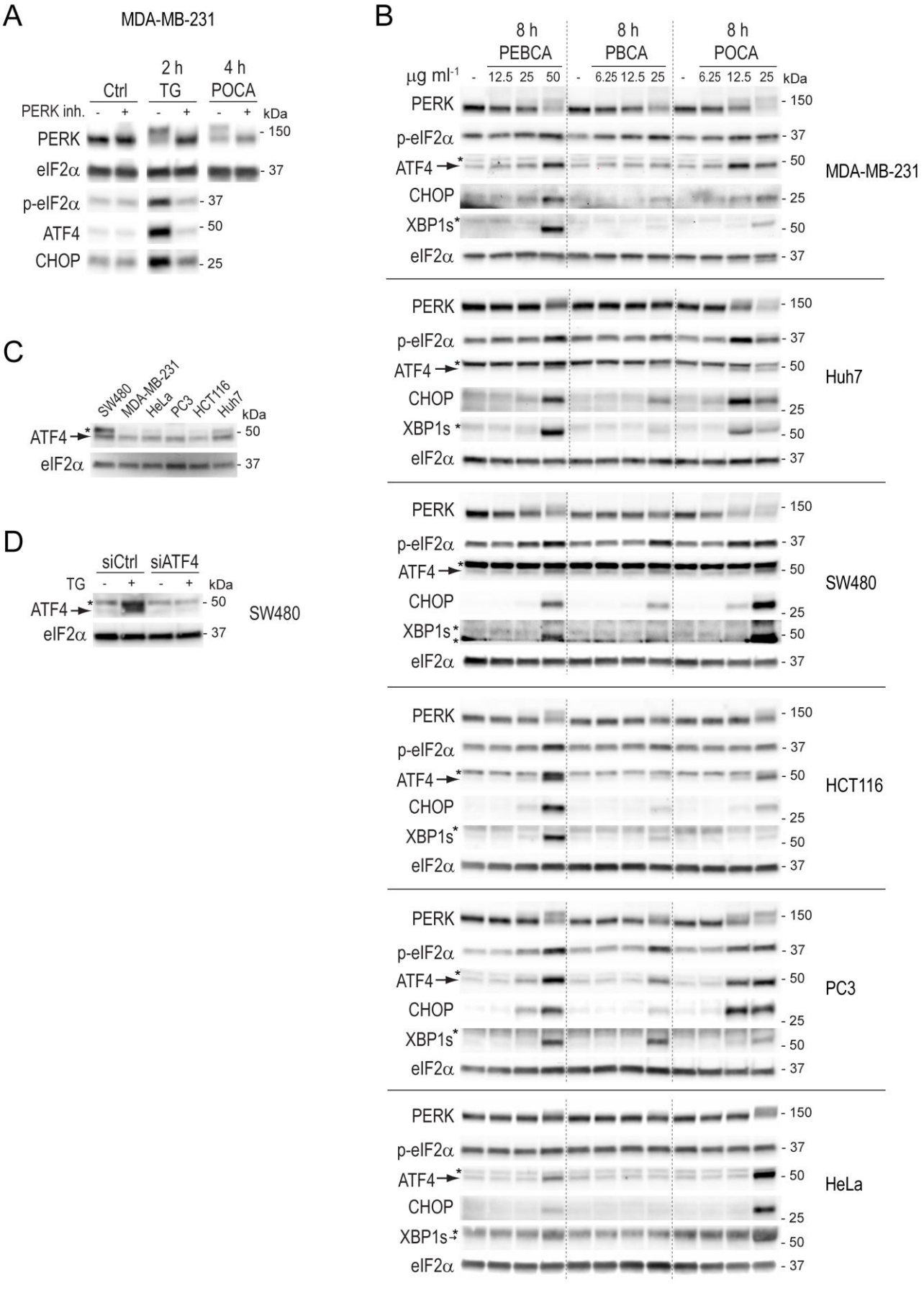

Supplementary Figure 2. The PACA particles differentially induce ER stress. A. To verify the specificity of the upward bandshift of PERK as readout for PERK activation and demonstrate the downstream signaling in the PERK pathway, MDA-MB-231 cells were treated with the well-known ER stressor thapsigargin (TG, 100 nM, 2 hours) or POCA particles (25 µg ml^{-1}, 4 hours) in the absence or presence of the PERK inhibitor GSK2606414 (100 nM). Cell lysates were prepared for immunoblotting and the blots were probed with the indicated antibodies. Inhibition of PERK totally abolished the TG-induced bandshift of PERK, the phosphorylation of eIF2α and accumulation of ATF4. Also POCA-induced PERK activation was abolished by the PERK inhibitor. **B.** The panel of cell lines was treated with the indicated concentrations of PEBCA, PBCA and POCA particles for 8 hours. At these concentrations cell death was kept to a minimum, except for 25 µg ml^{-1} of POCA particles. Cell lysates, including detached cells, were prepared for immunoblotting. The blots were probed with the indicated antibodies. In blots of ATF4 and XBP1s the asterisks denote unspecific bands. All samples were compared side by side on the same gel; the vertical dotted lines are drawn to simplify comparison. **C**. The unspecific band appearing on ATF4 immunoblots was compared across our panel of cell lines by immunoblotting of equal amounts of cell lysate. **D**. The upper band on ATF4 immunoblots was identified as unspecific by siRNA-mediated depletion of ATF4 in SW480 cells. Two days after transfection with either non-targeting control siRNA (siCtrl) or siRNA specific for ATF4, the cells were stimulated by TG (100 nM, 4 hours) before lysates were prepared for immunoblotting. Only the lower band was specifically depleted by siATF4.

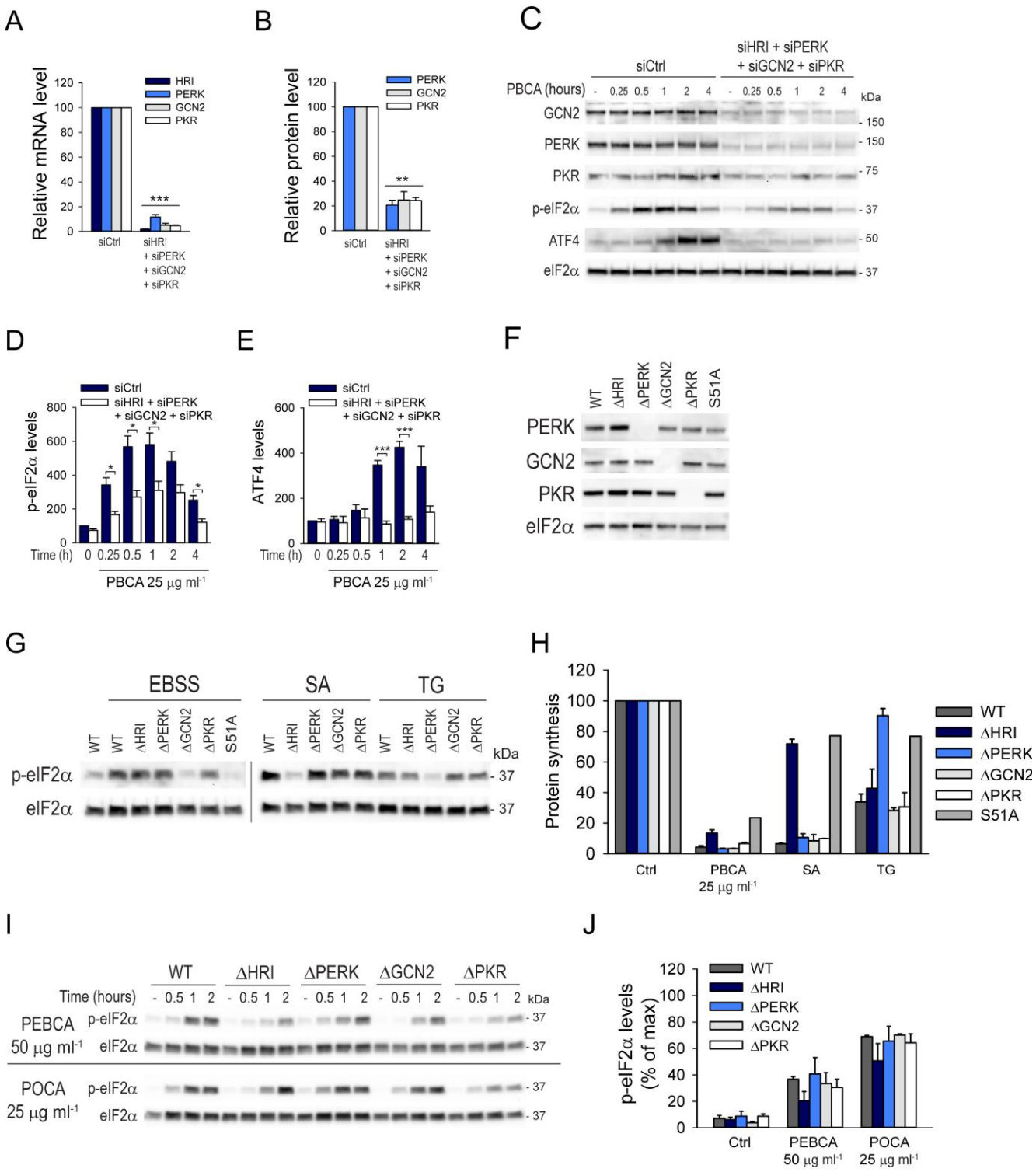

Supplementary Figure 3. The PACA particles differentially activate the integrated stress response. The efficiency of the simultaneous knockdown of the four integrated stress response kinases GCN2, PERK, HRI, and PKR was determined at the mRNA level for all four kinases (**A**) and at the protein level for the three kinases with commercially available antibodies (**B**). The asterisks denote the statistical significances compared to the untreated control. **C-E**. MDA-MB-231 cells were transfected with non-targeting control siRNA or a

mixture of siRNAs targeting the four ISR kinases. After 48 hours the cells were treated with PBCA particles (25 µg ml^{-1}) for the indicated times and cell lysates were prepared for immunoblotting. The relative levels of p-eIF2α (D) and ATF4 (E) were normalized to total eIF2α. **F**. Lysates of HAP1 WT, ΔGCN2, ΔPERK, ΔPKR, ΔHRI, and S51A cells were assessed for expression of GCN2, PERK, and PKR by immunoblotting. **G**. Functional knockout of GCN2, HRI and PERK in the HAP1 cells were assessed by starving the cells for amino acids in Earles's balanced salt solution (EBSS, 1 hour), inducing oxidative stress by sodium arsenite (SA, 200 µM, 1 hour), or inducing ER stress by thapsigargin (TG, 4 µM, 2 hours), respectively. In S51A mutant eIF2α cells none of these stimuli activated p-eIF2α (only data for EBSS are shown). **H**. Relative protein synthesis measured by incorporation of [^{3}H]leucine for 20 minutes after treatment of the indicated HAP1 cells with PBCA particles (25 µg ml^{-1}, 1 hour). Treatment with sodium arsenite (200 µM, 1 hour), or thapsigargin (4 µM, 2 hours) served as positive controls for HRI and PERK, respectively. **I**. HAP1 WT, ΔHRI, ΔPERK, ΔGCN2, or ΔPKR cells were treated with PEBCA (50 µg ml^{-1}) or POCA (25 µg ml^{-1}) for the indicated times and cell lysates were prepared for immunoblotting. **J**. The ratio of p-eIF2α to total eIF2α was normalized to the maximum intensity within each experiment (instead of normalization to Ctrl) since the basal level of p-eIF2α was very low in these cells. The maximum p-eIF2α level was obtained by PBCA-treatment (data shown in Figure 2H). All bars show mean values ± SEM quantified from at least three independent experiments, except in H. where mean values from 2 independent experiments are presented as percent of untreated control, and the error bars denote the deviation from mean. *, $p < 0.05$; **, $p < 0.01$; ***, $p < 0.001$.

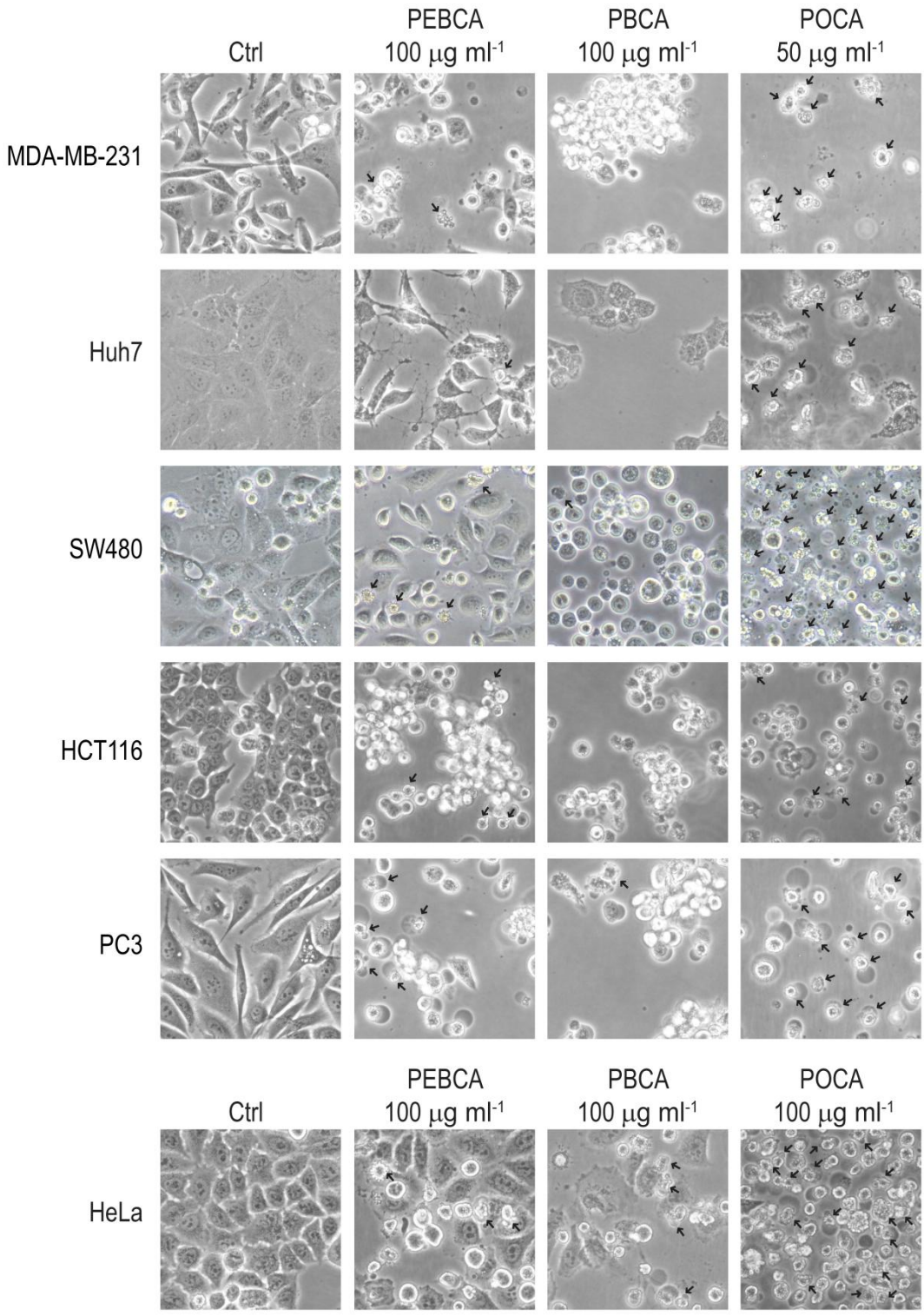

Supplementary Figure 4. POCA particles induce apoptotic phenotypes across a panel of cell lines. Phase contrast images of MDA-MB-231, Huh7, SW480, HCT116, PC3, and HeLa cells treated with 50 or 100 μg ml^{-1} of PEBCA, PBCA or POCA particles, as indicated, for 24 hours. Arrows indicate examples of condensed cells with extensive blebbing.

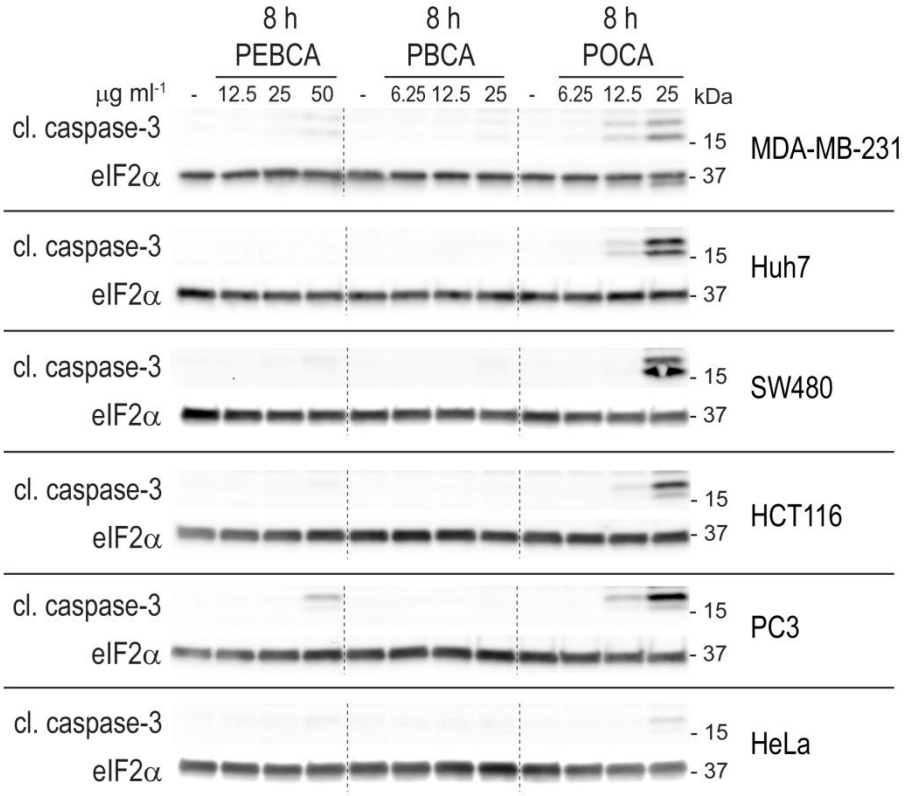

Supplementary Figure 5. POCA particles induce cleavage of PARP and caspase-3 across a panel of cell lines. The indicated cell lines were treated with the indicated concentrations of PEBCA, PBCA or POCA particles for 8 hours and cell lysates, including detached cells, were prepared for immunoblotting. The blots were probed with antibodies against cleaved caspase-3 (cl. caspase-3) and eIF2α.

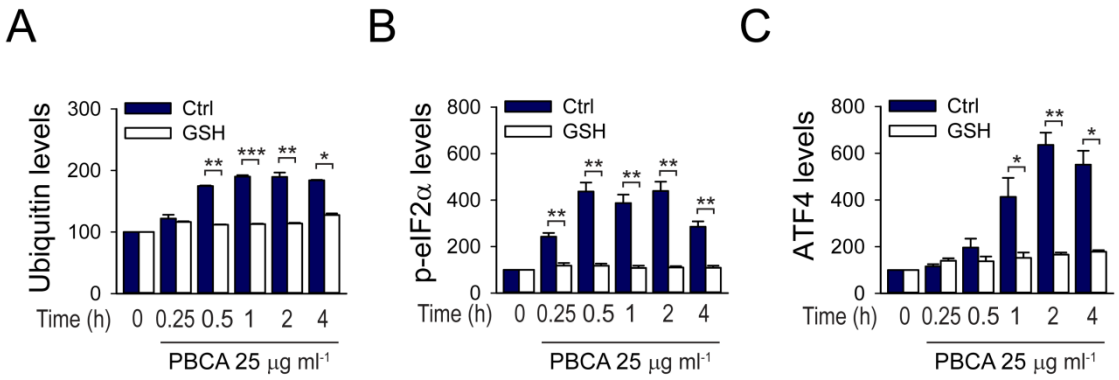

Supplementary Figure 6. Excess glutathione inhibits the PBCA-induced stress responses in MDA-MB-231 cells. MDA-MB-231 cells were treated with PBCA (25 μg ml^{-1}) in the absence or presence of reduced glutathione (GSH, 10 mM) for the indicated times and lysates were prepared for immunoblotting. The relative levels of ubiquitin (**A**), p-eIF2α (**B**), and ATF4 (**C**) were normalized to total eIF2α. The bars show mean values ± SEM quantified from at least three independent experiments. *, $p < 0.05$; **, $p < 0.01$; ***, $p < 0.001$.

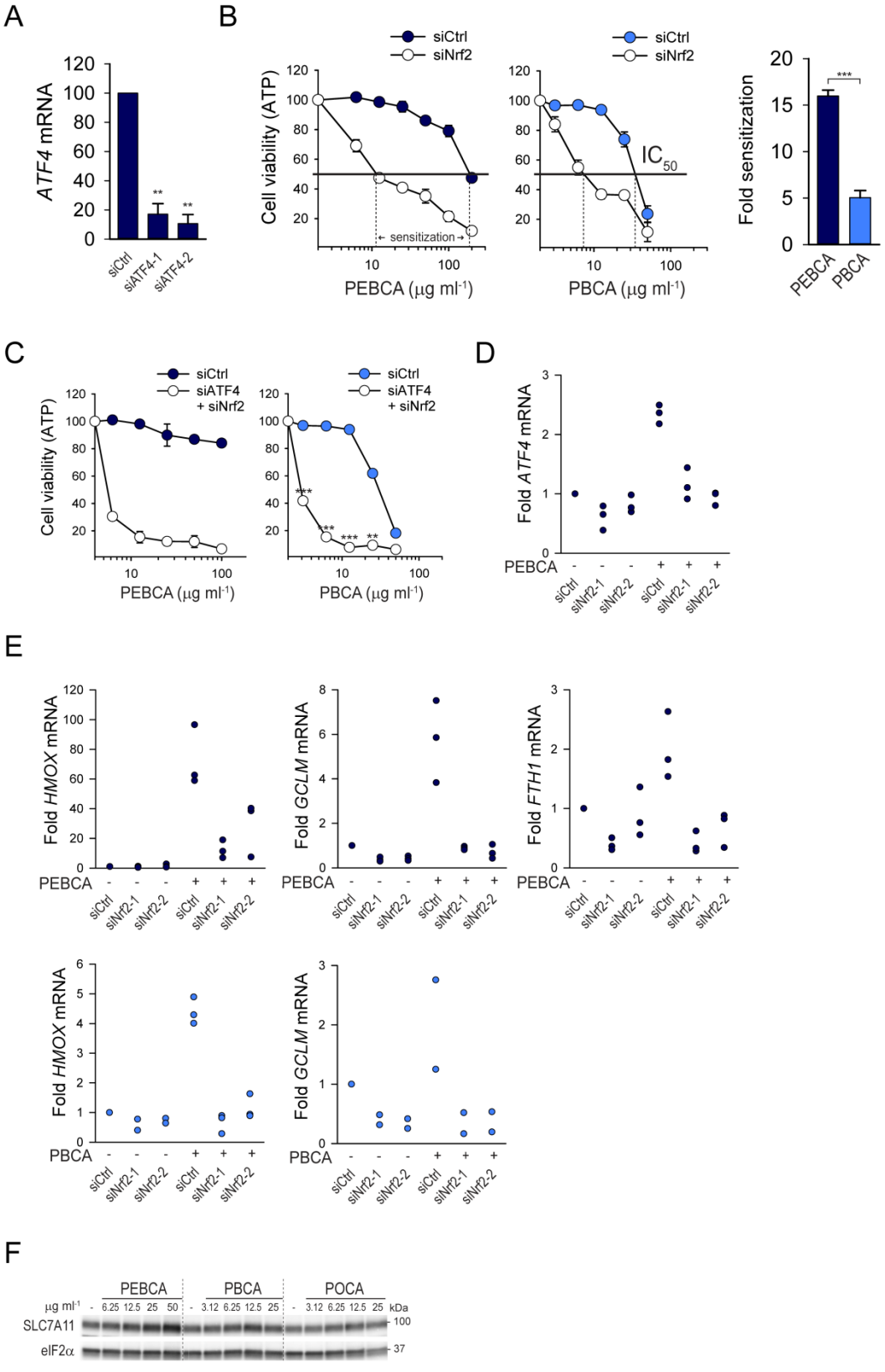

Supplementary Figure 7. ATF4 and Nrf2 mediate protection against PEBCA- and PBCA cytotoxicity in MDA-MB-231 cells. A. Knockdown efficiency of *ATF4* mRNA in MDA-MB-231 cells transfected with a non-targeting control siRNA (siCtrl) or two

independent siRNAs against ATF4. The asterisks denote the statistical significances compared to the untreated control. **B**. To assess the impact of Nrf2 depletion on cell viability, fold sensitization to PEBCA or PBCA particles was calculated in cells depleted for Nrf2 (by siNrf2-2). To this end, IC_{50} values (the concentration of particles that induced 50% reduction in cell viability, indicated by dotted lines) were calculated for siCtrl and siNrf2 in each experiment that together make up Figure 6C. The fold sensitization is given as the IC_{50} ratio between siCtrl and siNrf2. **C**. Cell viability assessed as ATP levels of MDA-MB-231 cells depleted for both Nrf2 and ATF4 and 48 hours later treated with PEBCA or PBCA particles for 24 hours. The data were normalized to the respective non-particle-treated control. Double depletion of ATF4 and Nrf2 in itself only reduced the viability of untreated control cells by ~20%. The asterisks denote the statistical significance between siCtrl and siATF4 + siNrf2 for each concentration of PBCA. The curves were extended to 100% viability to simplify comparison between siCtrl and siATF4 + siNrf2. **D**. *ATF4* mRNA levels in MDA-MB-231 cells transfected with a non-targeting control siRNA (siCtrl) or two independent siRNAs against Nrf2, and then 48 hours later treated with PEBCA particles (50 µg ml^{-1}) for 4 hours. **E**. mRNA levels of *HMOX*, *GCLM* or *FTH1* in cells transfected with a non-targeting control siRNA (siCtrl) or by two independent siRNAs targeting Nrf2. 48 hours later the cells were treated with PEBCA (50 µg ml^{-1}) or PBCA (12.5 µg ml^{-1}) for 4 hours. **F**. MDA-MB-231 cells were treated with the indicated concentrations of PEBCA, PBCA or POCA for 16 hours and cell lysates were prepared for immunoblotting. All graphs show mean values ± SEM quantified from at least three independent experiments, except Fig. S6B PEBCA (n=2) and 6D *GCLM* mRNA PBCA (n=2). *, $p < 0.05$; **, $p < 0.01$; ***, $p < 0.001$.

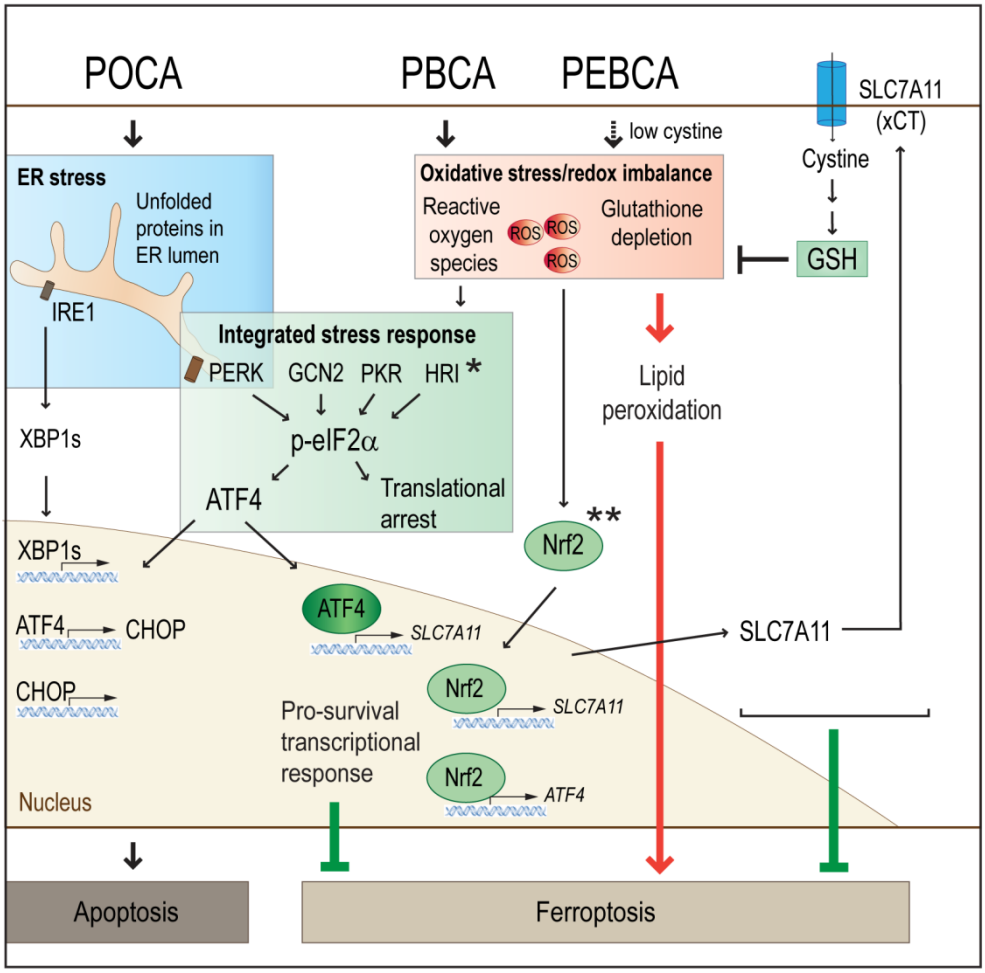

Supplementary Figure 8. Model for PACA-induced cellular stress responses and mode of cell death. This illustration highlights our most important findings. * HRI is particularly induced by PBCA. ** Nrf2 is particularly induced by PEBCA. The POCA particles are the most potent inducers of ER stress, both via the PERK pathway and the IRE1 pathway. They are also the most potent inducers of apoptosis. At high concentrations the PEBCA particles induce ER stress and accumulation of ATF4, but concomitantly they potently induce pro-survival Nrf2 activation and downstream transcription of the cystine transporter *SLC7A11*. PBCA particles only weakly activate ER stress, but rather induce oxidative stress that is sensed by heme-regulated eIF2α kinase (HRI) and leads to accumulation of ATF4. PBCA particles also activate Nrf2, and both ATF4 and Nrf2 are responsible for the pro-survival PBCA-induced transcription of *SLC7A11*. PBCA particles deplete the cells of GSH and induce the lipid peroxidation-dependent cell death pathway ferroptosis. PEBCA particles induce ferroptosis if the availability of cystine is low.